Natural and Applied Sciences International Journal (NASIJ)
eISSN: 2788-4619 (online)
https://ideapublishers.org/index.php/nasij
Vol. 6, No. 1 (January-June), 2025, pp. 29-58
https://doi.org/10.47264/idea.nasij/6.1.2
Original Research Article

Multi-satellite analysis of key climate variables over Qinghai province: GNSS-RO vs remote sensing (2019–2023)

Asma Sajid*[1] | Syed Faizan Haider[2]

1. Department of Space Science, Institute of Space Technology, Islamabad, Pakistan.
2. Nexus Next Cost Company, Brussels, Belgium.

* Corresponding Author Email: asmasajidist@gmail.com

Abstract: Reliable climate monitoring is essential for understanding environmental changes in sensitive regions such as Qinghai province, China, where complex topography and scarce ground observations challenge accurate assessment. In this context, GNSS-RO has emerged as a robust technique, offering high vertical resolution, global coverage, and long-term stability. This study conducts a comparative analysis of three key climate variables: air temperature, precipitation, and evapotranspiration in Qinghai from 2019-2023 using GNSS-RO alongside widely used satellite-based datasets, namely ERA5 for air temperature, GPM for precipitation, and TerraClimate for evapotranspiration. Results reveal notable discrepancies: remote sensing air temperatures (269.56–271.69 K) were consistently higher than GNSS-RO values (~263.2 K); TerraClimate evapotranspiration estimates (2,600– 2,734 mm) were substantially larger than GNSS-RO values (~500 mm/year); and GNSS-RO precipitation outperformed GPM with lower bias and RMSE (2.130 mm; 5.900 mm vs. 18.573 mm; 22.601 mm). These differences may reflect the influence of regional topography, atmospheric variability, and dataset-specific retrieval methods. Spatiotemporal variations were especially evident in high-altitude areas, underscoring GNSS-RO's advantage in capturing mountain climate dynamics. Overall, the findings emphasise the need for integrating multiple satellite platforms to reduce uncertainties, strengthen climate monitoring in data-scarce regions, and provide more reliable evidence for climate policy and future adaptation strategies.

Article History

Received:
16-Apr-2025

Revised:
15-May-2025

Re-revised:
20-Jun-2025

Accepted:
22-Jun-2025

Published:
30-Jun-2025

Keywords: Spatiotemporal analysis, Data-scarce environments, Satellite data integration, Evapotranspiration assessment, Precipitation, Climate adaptation strategies.

How to Cite: Sajid, A. & Haider, S. F. (2025). Multi-satellite analysis of key climate variables over Qinghai province: GNSS-RO vs remote sensing (2019–2023). *Natural and Applied Sciences International Journal (NASIJ), 6*(1), 29-58. https://doi.org/10.47264/idea.nasij/6.1.2

1. Introduction

Global Navigation Satellite Systems (GNSS) have evolved beyond their original use in positioning to become powerful tools for atmospheric monitoring. Their signals, which can penetrate through clouds and weather systems, provide continuous, all-weather, and near-real-time data. Using radio occultation, GNSS enables accurate retrieval of atmospheric parameters such as water vapour, temperature, and pressure, making it an important technique for climate research (Jin & Komjathy, 2010).

Qinghai province, located in the northeastern part of the Qinghai-Tibet Plateau, functions as a critical ecological barrier with substantial influence on regional and national environmental systems (An *et al.*, 2024). As a high-altitude, ecologically sensitive region, it has been increasingly affected by climate change, with rising temperatures, shifting precipitation patterns, and heightened vulnerability to extreme weather events (Zhang *et al.*, 2023).

The Tibetan Plateau (TP), often referred to as the "third pole" serves as a critical zone of interaction among the atmosphere, cryosphere, hydrosphere, and biosphere. Qinghai province, situated in the northeastern part of the TP, is directly linked to this system and contains the headwaters of several of Asia's major rivers, providing essential water resources that sustain downstream populations and economic activities. However, over the past three decades, the TP has experienced marked climatic changes that have altered atmospheric and hydrological cycles, leading to shifts in river discharges, the expansion of glacier-fed lakes, and widespread permafrost degradation. These transformations threaten regional water security, ecosystems, and livelihoods, while future projections warn of reduced downstream water availability under continued warming (Yang *et al.*, 2014).

Atmospheric climate monitoring requires observations of consistently high quality that meet the standards set by the Global Climate Observing System (GCOS). Since 2001, radio occultation (RO) data derived from GPS signals have been provided by multiple satellite missions, offering global coverage, high accuracy, and satisfactory vertical resolution in the troposphere and lower stratosphere. Importantly, structural uncertainty in climate trends is lowest between 8 and 25 km altitude across all RO missions and variables. For temperature, uncertainties remain below 0.05 K per decade in the global mean and below 0.1 K per decade at all latitudes (Steiner *et al.*, 2020).

Qinghai's ecological significance and sensitivity to climatic changes, broader efforts in climate monitoring and analysis become increasingly essential. Effective climate change monitoring and analysis are integral to understanding environmental dynamics and require the systematic examination of both spatial and temporal variability (Sa'i *et al.*, 2024). Climate monitoring, prediction, and research are fundamental pillars of the global strategy to mitigate and adapt to climate change. Improved accuracy in assessing the pace of climate change, along with a more precise characterisation of associated uncertainties, can enhance policy formulation and potentially expedite the establishment of a global consensus on climate action (Moses *et al.*, 2023). To better understand the significance of these impacts, it is essential to examine the region's specific climatic features. Low temperatures, long hours of sunshine, and intense solar radiation characterise the region's climate. The annual mean temperature ranges between 0°C and 3.4°C. Precipitation is primarily concentrated between July and September, with annual rainfall varying from approximately 273.7 mm to 467.8 mm. Since the 1960s, the region's temperature has been rising at a rate of about 0.25°C per decade. This increase is higher than

the warming seen in other regions at similar latitudes (Zhu *et al.*, 2024) In response to the limitations of ground-based observations in regions like Qinghai, satellite-based technologies have become essential tools for climate assessment. Satellite remote sensing has made significant advances in understanding the climate system and its changes by quantifying atmospheric, land, and ocean processes and spatiotemporal states (Yang *et al.*, 2013).

Remote sensing has emerged as an increasingly vital component of contemporary climate research. The continual expansion of long-term satellite-derived datasets has provided robust evidence for detecting and quantifying changes and trends within the global climate system. Moreover, advancements in sensor technology and measurement methodologies have substantially enhanced the precision and resolution of observations, enabling the retrieval of detailed information on key climatic variables. These developments contribute critical inputs to climate modelling and simulation frameworks, thereby improving the accuracy and reliability of climate projections (Cracknell & Varotsos, 2011).

The accuracy and reliability of GNSS-RO for retrieving atmospheric parameters such as temperature, pressure, and water vapour have been well established in earlier studies (Anthes *et al.*, 2008; Kursinski *et al.*, 1997; Yu *et al.*, 2014). Comparative analyses with AIRS and other satellite systems confirmed its superior vertical resolution and global coverage (Kursinski & Hajj, 2001; Wulfmeyer *et al.*, 2015). In high-altitude and data-sparse regions such as the Qinghai–Tibet Plateau, GNSS-RO has shown particular promise for capturing fine-scale atmospheric variability (Ding *et al.*, 2022; Zhao *et al.*, 2021). However, limited research has systematically compared GNSS-RO derived variables with conventional remote sensing and reanalysis products over Qinghai Province. Among GNSS techniques, radio occultation has proven to be a powerful indirect method for observing atmospheric profiles in both the upper and lower regions of the atmosphere (Moses *et al.*, 2023). The GNSS-RO technique provides globally distributed, all-weather observations with high vertical resolution, exceptional measurement accuracy, and long-term stability, making it particularly effective for profiling the middle and upper troposphere, stratosphere, and ionosphere (Moses *et al.*, 2023).

GNSS-RO refers to the transmission of signals from GNSS satellites to Low Earth Orbit (LEO) satellites, such as COSMIC, GRACE, METOP, and CHAMP, with the signals passing through the Earth's atmosphere prior to reception (Sa'i *et al.*, 2024). It relies on the continuous transmission of radio signals from GNSS satellites (GPS/GLONASS/Galileo), which orbit Earth at approximately 20,000 km above the surface (Sa'i *et al.*, 2024). This technique measures the refraction of GNSS signals through the atmosphere during satellite occultation events, providing high vertical-resolution, cloud-independent profiles from the surface to the upper stratosphere. Its long-term stability and global coverage make it highly valuable for climate monitoring and model evaluation (Gleisner *et al.*, 2022).

GNSS-RO has become one of the most accurate and dependable techniques for atmospheric profiling, offering distinct advantages over conventional observation methods used in numerical weather prediction (NWP) and climate analysis. At leading NWP centres, its data are assimilated using advanced observation operators such as the RO Processing Package (ROPP), providing critical input for both global and regional analyses. Owing to its exceptional precision and long-term stability in the upper troposphere and lower stratosphere (UT/LS), it provides more reliable, bias-free information than traditional satellite or radiosonde measurements. Assimilation of bending-angle (α or BA) profiles has been shown to

substantially enhance forecasting skill by improving temperature and humidity retrievals and by aiding radiance bias correction. Moreover, recent Observing System Simulation Experiments (OSSEs) demonstrate that expanding global coverage continues to improve forecast accuracy, highlighting the method's unique capacity to provide high-resolution, all-weather, and globally consistent atmospheric observations that surpass the limitations of traditional systems (Wu *et al.*, 2024)

Building on the demonstrated strengths of GNSS-RO, this study further explores the integration of satellite-based remote sensing datasets to provide a comprehensive evaluation of climate variables. The ongoing advancement of remote sensing technologies, including next-generation satellite systems and innovative large-scale data processing techniques, is critical for enhancing the precision and reliability of climate change research that relies on remotely sensed data (Wang, 2023). The meteorological variables were acquired from multiple satellite-based remote sensing datasets. Air temperature data were obtained from the fifth-generation ECMWF Reanalysis (ERA5), precipitation measurements were sourced from the Global Precipitation Measurement (GPM) mission, and evapotranspiration data were extracted from the TerraClimate dataset. All remote sensing datasets were accessed and processed through the Google Earth Engine platform. These remote sensing-derived parameters were subsequently compared with corresponding data obtained via radio occultation to assess their consistency and accuracy. Each of these variables reflects distinct but interconnected aspects of atmospheric and surface processes, making them ideal for satellite-based climate evaluation.

Air temperature represents one of the most critical and direct indicators of climate change. It serves as a fundamental variable in the analysis of climate dynamics, hydrological processes, ecological transformations, and disaster risk assessment. In recent years, the persistent increase in air temperatures has been closely associated with the heightened intensity and frequency of extreme weather events, including heatwaves and severe droughts (Zhang *et al.*, 2024).

Closely linked to temperature dynamics, precipitation exhibits variability on interannual and decadal scales, with changes in its amount, intensity, frequency, and form (e.g., snow versus rain) exerting significant impacts on both the environment and society. Increasing evidence indicates that anthropogenic climate change, particularly global warming, is altering precipitation patterns and intensifying the hydrological cycle, with pronounced effects on extreme weather events (Trenberth, 2011).

Complementing the roles of temperature and precipitation, evapotranspiration is a critical process studied across multiple disciplines, including hydrology, agriculture, energy balance, and climate science. It plays a vital role in determining irrigation requirements and estimating surface runoff, contributes to the assessment of the Earth's surface energy budget, enhances the accuracy of atmospheric circulation models, and is essential in the characterisation of climatic conditions (Ajjur & Al-Ghamdi, 2021).

Despite the increasing availability of satellite-based climate datasets such as GPM, ERA5, and TerraClimate, their performance in high-altitude and topographically complex regions like Qinghai province remains inadequately validated (Liu *et al.*, 2023; Sun *et al.*, 2023). Most existing studies have focused on large-scale or lowland regions, often overlooking the unique climatic variability and retrieval limitations present in mountainous terrains (Steiner *et al.*, 2013). Furthermore, there is a notable scarcity of research comparing vertical atmospheric profiles from GNSS-RO data with surface-level remote sensing products across identical

spatial and temporal domains. This lack of integrated analysis constrains our understanding of climate trends in ecologically sensitive areas such as the Qinghai–Tibet Plateau. Addressing this gap is essential for improving the accuracy and consistency of satellite-derived climate indicators in complex topographies.

Previous research has highlighted the considerable potential of GNSS-RO and satellite-based remote sensing in monitoring climate variability across the Qinghai-Tibet Plateau. Nevertheless, significant discrepancies have been observed among different satellite products, particularly in temperature and evapotranspiration estimates over high-altitude and topographically complex regions (Peng *et al.*, 2016; Tran *et al.*, 2023). These inconsistencies are primarily attributed to differences in spatial resolution, retrieval algorithms, and atmospheric correction approaches (Vannah *et al.*, 2025). However, limited effort has been devoted to systematically investigating the underlying causes of these variations or assessing their broader implications for climate modelling, data assimilation, and policy development in the region.

Despite these technological advancements, significant research gaps remain in evaluating the consistency and performance of GNSS-RO and remote sensing datasets in high-altitude, topographically complex regions such as Qinghai province, China. These ecologically sensitive areas are increasingly vulnerable to the impacts of climate change, underscoring the urgent need for accurate and consistent climate observations. However, the scarcity of dense ground-based observational networks in these areas poses significant challenges for accurate climate monitoring. This study is motivated by the need to improve the reliability of climate data in complex terrain by evaluating GNSS-RO and satellite-based remote sensing datasets. It addresses both the scientific imperative to validate satellite-derived climate variables and the broader societal need for robust climate analysis tools in environmentally sensitive, data-scarce regions. To address these scientific gaps, this study sets out with the following objectives:

- To compare GNSS-RO and satellite-based datasets (GPM, ERA5, TerraClimate) for climate variable estimation over Qinghai Province.
- To analyse spatiotemporal trends in air temperature, precipitation, and evapotranspiration from 2019 to 2023.
- To assess the consistency and reliability of GNSS-RO data relative to remote sensing products in a complex topographical setting.

2. Materials and methods

2.1. METOP

Since 2007, the Meteorological Operational (MetOp) satellite series, operated by the European Organisation for the Exploitation of Meteorological Satellites (EUMETSAT), has provided long-term observations of the Earth's surface and atmosphere to support meteorological operations and climate research. Although primarily designed for weather forecasting, MetOp delivers key climate-relevant products, such as tropospheric temperature and water vapour profiles derived from infrared and microwave sounders (Trent *et al.*, 2023).

The satellites operate in a polar, sun-synchronous orbit at an altitude of approximately 817 km and an inclination of 98.7°, ensuring consistent local-time observations. Each orbit takes about 101 minutes, enabling over 14 orbits per day and near-global coverage. The mission’s objective

is to deliver reliable long-term datasets to support forecasting and global climate monitoring (Clerbaux *et al.*, 2009). In this study, MetOp data from 2019 to 2023 were programmatically extracted for Qinghai Province, China.

2.2. ERA5

The ERA5 reanalysis dataset, developed by the European Centre for Medium-Range Weather Forecasts (ECMWF), provides global climate data with a 31 km spatial and hourly temporal resolution, covering the period from 1950 to near real-time. ERA5 is widely recognised for its enhanced performance relative to other reanalysis products, owing to its finer resolution and improved data assimilation methods that include the latest satellite observations. Numerous validation studies have demonstrated the high consistency of ERA5-derived meteorological parameters with ground-based and remote sensing observations, confirming the dataset's reliability for climate analysis (Hassan *et al.*, 2024).

2.3. GPM

The Global Precipitation Measurement (GPM) mission, jointly led by NASA and JAXA, aims to unify and improve spaceborne global precipitation observations (Draper *et al.*, 2015). Operating in a non-sun-synchronous orbit at ~407 km, the GPM Core Observatory carries the GPM Microwave Imager (GMI) and Dual-frequency Precipitation Radar (DPR). GMI provides calibrated passive microwave observations and serves as the radiometric reference for the GPM constellation, while the mid-inclination orbit enables overlap with polar-orbiting radiometers, enhancing coverage (Newell *et al.*, 2015). The mission targets five key objectives: (a) improving precipitation data accuracy and coverage; (b) advancing knowledge of precipitation processes, water cycle variability, and freshwater distribution; and enhancing (c) hydrological, (d) climate, and (e) weather prediction systems (Skofronick-Jackson *et al.*, 2018).

2.4. TerraClimate

The terraClimate dataset, developed by researchers at the University of Idaho, provides high-resolution monthly climate data at ~4 km spatial resolution, supporting climate and ecological research through detailed spatial and temporal coverage (Hanchane *et al.*, 2023). It offers a comprehensive suite of variables, including evapotranspiration, temperature, and precipitation (Araghi *et al.*, 2023). TerraClimate integrates high-resolution climatological normals from the WorldClim dataset with coarser-resolution monthly time-series data using climatically aided interpolation. This yields a global dataset that includes key climate variables such as precipitation, maximum and minimum temperature, wind speed, vapour pressure, solar radiation, and evapotranspiration (Abatzoglou *et al.*, 2017).

3. Methodology

3.1. Study area

Qinghai province, located in western China (31.5°–39.3°N, 89.3°–103°E), spans approximately 724,000 km², making it the fourth-largest province in the country (Ke *et al.*, 2009). Positioned in the northeastern Qinghai–Tibetan Plateau, the region comprises three major topographic zones: the Qilian Mountains in the north, the Qaidam Basin in the centre, and the Southern Qinghai Plateau. Elevation ranges from 1,650 m (Minhe County) to 6,860 m

(Bukadaban Peak, Kunlun Mountains), with a mean elevation exceeding 3,000m. About 26.3% of the area lies below 3,000 m, 67% between 3,000 and 5,000 m, and 5% above 5,000 m. The higher elevations are dominated by extensive glaciers and permanent snow cover, while the central basin features semi-arid to arid desert and upland grassland ecosystems (Ke *et al.*, 2009). The average altitude of the study area exceeds 3,000 m, and the region experiences a continental plateau climate. The mean annual temperature ranges from −5.7 °C to 8.5 °C, and the annual total precipitation varies between 50 mm and 450 mm (Zhao *et al.*, 2021).

This region was selected for the present study due to its ecological vulnerability and clear indications of climate change, including increasing near-surface air temperatures, shifting precipitation regimes, and accelerating glacial retreat. These factors establish Qinghai as a key area for assessing climate variability, evapotranspiration processes, and ecological responses within semi-arid, high-altitude ecosystems.

Figure 1: The geographical location of Qinghai, China.

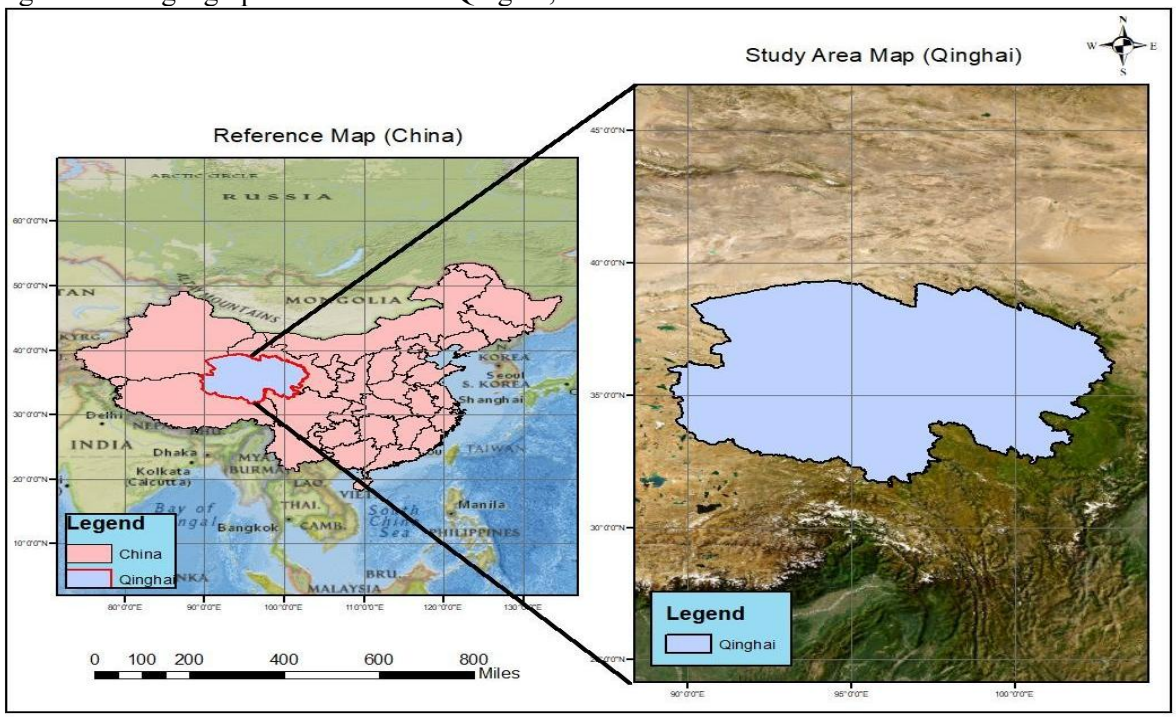

3.2. Data collection

Google Earth Engine (GEE) is a cloud-based platform developed by Google that enables large-scale geospatial analysis, visualisation, and processing of Earth science data, with a particular emphasis on satellite-based Earth observation datasets (Zhu *et al.*, 2024). GEE provides access to a vast array of geospatial datasets and satellite imagery, coupled with robust spatial analysis capabilities. Data retrieval on the GEE platform is highly efficient, typically requiring only a few lines of code, as it automates data loading and processing. Consequently, users do not need to perform manual radiometric or geometric corrections, as the platform handles them internally. Instead, users focus on scripting specific processing workflows tailored to their research objectives (Kazemi Garajeh *et al.*, 2024).

Using the GEE platform, remote sensing data relevant to evapotranspiration, air temperature, and precipitation were obtained from the TerraClimate, ERA5, and GPM datasets,

respectively. These datasets were selected based on their consistency, spatiotemporal resolution, and established reliability for climate change assessments. In parallel, radio occultation data for the same variables were retrieved from the MetOp (Meteorological Operational) satellite series through code-based access, enabling automated and efficient extraction of atmospheric profiles.

These satellite-derived observations are widely recognised for their accuracy and suitability in climate and hydrological research. Both remote sensing and radio occultation datasets focused on the Qinghai region and covered the period from 1 January 2019 to 31 December 2023. The acquired data were initially downloaded as GeoTIFFs and subsequently converted to CSVs to enable time-series extraction and statistical analysis via scripted processing, facilitating integration across data sources. Preprocessing steps were applied to ensure data quality, including the exclusion of anomalous values to enhance the robustness of subsequent analyses.

3.3. Data collection and processing criteria

The selection of satellite and GNSS-RO datasets was guided by their temporal coverage, spatial resolution, and proven reliability in representing key climate variables over high-altitude regions. TerraClimate was chosen for its high-resolution (4 km) monthly data on temperature and evapotranspiration; ERA5 for its globally consistent reanalysis-based air temperature fields; and GPM for its high-frequency precipitation estimates. These datasets have been widely validated for climate variability studies over the Qinghai–Tibet Plateau. (Zhao *et al.*, 2021; Li *et al.*, 2022). GNSS-RO data from the MetOp satellite series were selected due to their high vertical resolution and minimal bias, ensuring robust atmospheric profiling under varying conditions. Data spanning 2019–2023 were analysed to capture both interannual and seasonal variations in climatic parameters.

Prior to analysis, all datasets were resampled to a common spatial resolution and temporal frequency. The study area boundary was clipped to the Qinghai Province shapefile to ensure spatial consistency across all datasets.

3.4. Data validation and analysis

Validation was performed through cross-comparison between GNSS-RO and remote sensing datasets for overlapping temporal and spatial domains. Statistical performance metrics, including the Pearson correlation coefficient (r), root mean square error (RMSE), and mean bias error (MBE), were employed to evaluate the degree of agreement between datasets. Temporal averaging was used to minimise short-term fluctuations and enhance comparability. The analysis workflow was executed in both Google Earth Engine (GEE) and Python, leveraging libraries such as pandas, numpy, and matplotlib for time-series analysis and visualisation. Consistency checks were applied to identify and exclude outliers potentially arising from signal attenuation, retrieval errors, or missing observations.

3.5. Hinderances and validations

Despite the advantages of integrating GNSS-RO and remote sensing datasets, several challenges were encountered. The sparse spatial density of GNSS-RO observations limits detailed spatial pattern analysis, while remote sensing retrievals are occasionally affected by cloud contamination, surface emissivity variability, and retrieval algorithm assumptions.

Additionally, Qinghai's complex topography introduces orographic effects and localised atmospheric gradients that may influence temperature and precipitation measurements. These factors, though mitigated through averaging and cross-validation, introduce a degree of uncertainty into comparative analysis. Future work could incorporate in-situ meteorological observations to strengthen dataset validation.

4. Results

4.1. Precipitation analysis

4.1.1. Statistical performance metrics

Our comparison of precipitation data between GPM (satellite-based) and METOP (GNSS derived) datasets revealed substantial differences in statistical performance metrics, as illustrated in Figure 2a and 2b. Figure 2a shows the GPM-derived precipitation data, which display noticeably higher bias and error values, while Figure 2b presents the METOP data, reflecting lower error and greater temporal stability. Specifically, the GPM dataset exhibited considerably higher values for bias (18.6 mm) and MAE (18.5 mm) compared to METOP (2.1 mm for both metrics). The RMSE was also significantly higher for GPM (22.7 mm) than for METOP (5.9 mm), indicating that GNSS-derived precipitation estimates more closely align with expected climatological patterns.

Similarly, the unbiased RMSD (UbRMSD) and standard deviation (SD) were lower for METOP (5.5 mm) compared to GPM (12.6 mm), further confirming that the GNSS-derived approach provides more consistent and stable precipitation estimates over Qinghai Province.

Figure 2 (a & b): Statistical performance metrics for precipitation data (2019–2023) from GPM (top) and METOP (bottom) satellites

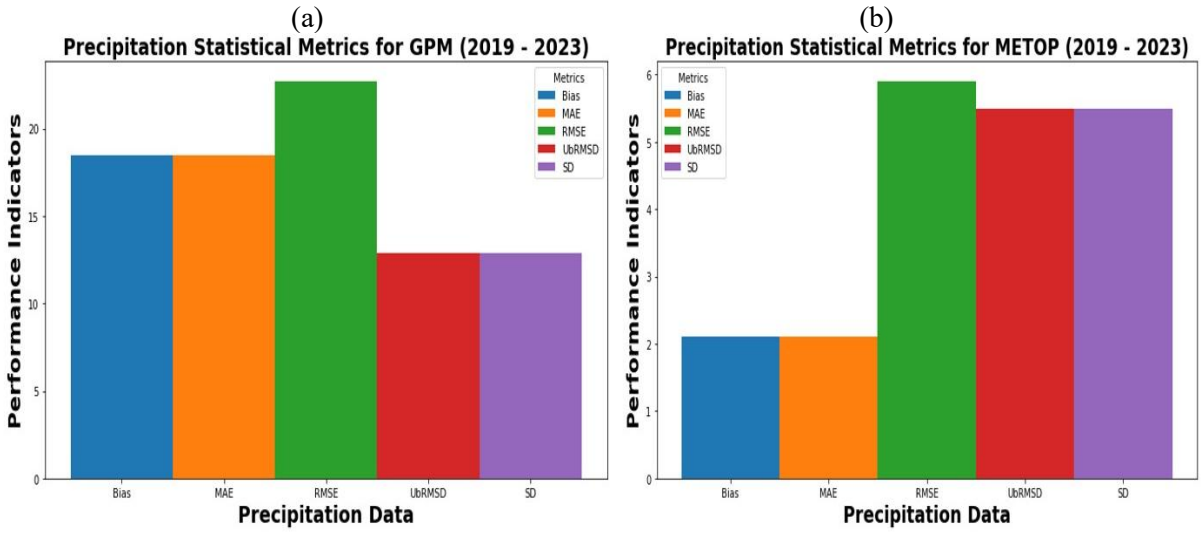

4.1.2. Temporal variations

The yearly average precipitation variations illustrated in Figure 3 revealed notable differences between the two products. As shown in Figure 3, GPM displays significant interannual fluctuations with visible peaks and troughs across the study period, whereas METOP maintains a nearly flat and stable trend line. GPM showed substantial interannual variability with

precipitation estimates ranging from 15.98 mm (2022) to 22.87 mm (2020), representing a variation of approximately 43%. In contrast, METOP exhibited remarkable stability across the five-year period, with values consistently around 2.13 mm (±0.01 mm), indicating minimal interannual variability. This visual contrast in Figure 3 highlights how GPM's variability likely reflects the influence of large-scale atmospheric dynamics, while METOP's consistent trend underscores the potential of GNSS-derived data for stable, long-term regional climate monitoring.

Figure 3: Yearly average precipitation values (2019–2023) obtained from GPM (top) and METOP (bottom) satellites

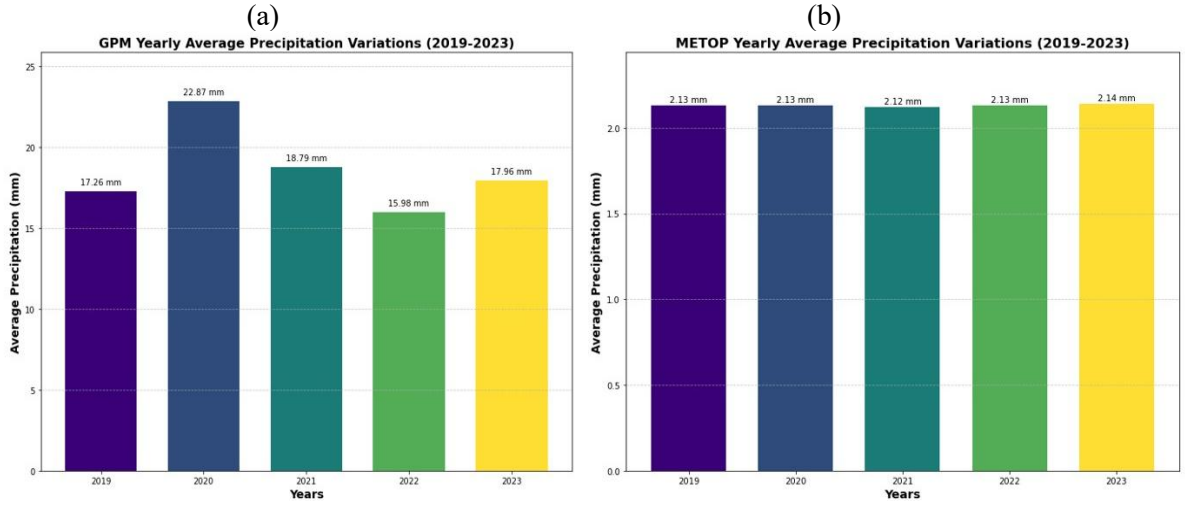

4.1.3. Seasonal variability

The analysis of seasonal precipitation patterns illustrated in Figure 4 revealed distinct variations between the two datasets. As depicted in Figure 4a, GPM displays a sharp seasonal cycle with high peaks during the summer months and a steep decline toward winter, while Figure 4b shows that METOP follows the same general pattern but at much lower magnitudes. GPM precipitation showed pronounced seasonal variability, with peak values occurring during the summer months (June–August) reaching approximately 40–45 mm, and minimum values during winter months (December–February) below 5 mm. This pattern reflects a distinct unimodal seasonal distribution, with peak precipitation coinciding with the summer monsoon period.

Figure 4: Yearly average precipitation variations from 2019 to 2023 derived from GPM (a) and METOP (b) satellite data

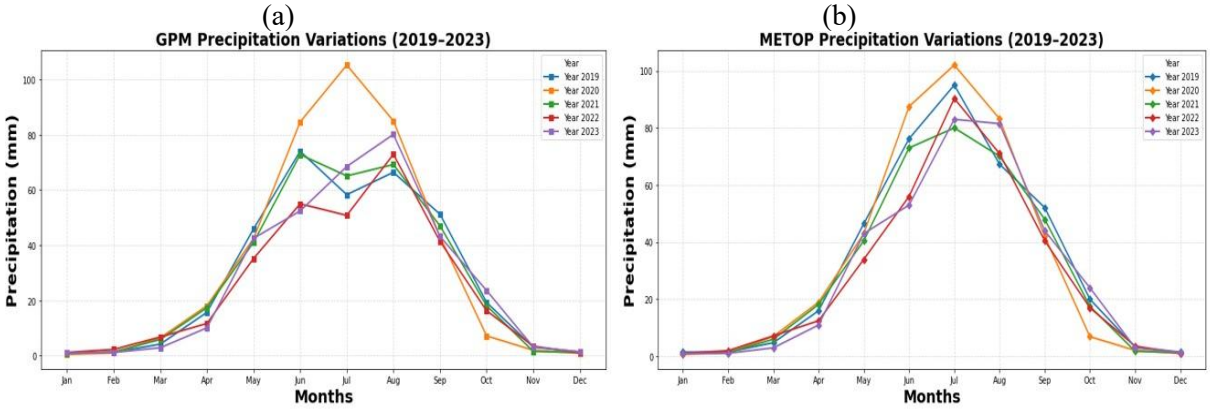

In contrast, Figure 4b highlights METOP's subdued amplitude, with summer peaks of around 6– 8 mm and near-zero precipitation during winter, emphasising its overall stability and lower magnitude. Both datasets consistently demonstrate the characteristic dry-winter and wet-summer pattern typical of the Qinghai region's continental climate.

4.1.4. Spatial distribution analysis

The contour and spatial analyses of GPM-derived precipitation data from 2019 to 2023 (as illustrated in Figure 5) reveal a consistent northwest-to-southeast gradient across Qinghai Province. Figure 5a displays the contour maps showing the broad precipitation distribution patterns, while Figure 5b provides detailed spatial maps highlighting local variations. Higher precipitation levels are consistently concentrated in the northwestern regions (shown in red/orange), with values gradually decreasing toward the southeastern areas (shown in blue). This spatial pattern remains remarkably stable across all five years, despite interannual variations in precipitation intensity. The contours presented in Figure 5a emphasise the smooth and coherent transition of precipitation zones, capturing large-scale regional gradients, whereas the finer spatial resolution in Figure 5b reveals localised intensity differences within the province. Both representations collectively demonstrate the strong spatial coherence captured by GPM satellite observations, with the gradient pattern consistently showing maximum precipitation in the northwestern portion of the province and minimum values in the southeastern regions.

Figure 5: GPM-based precipitation contours and spatial distribution across Qinghai, China

(a)

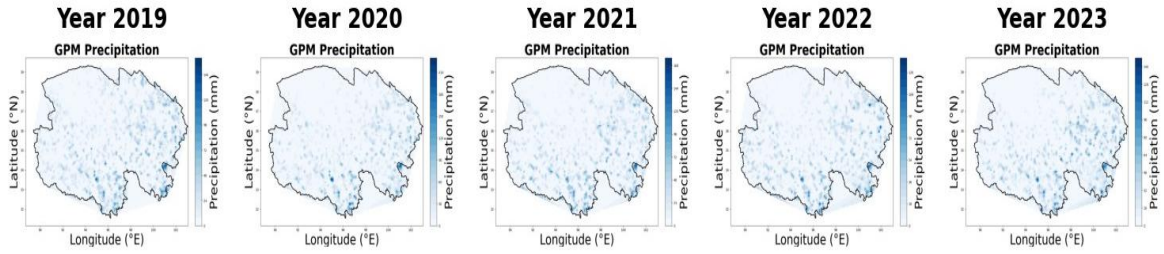

(b)

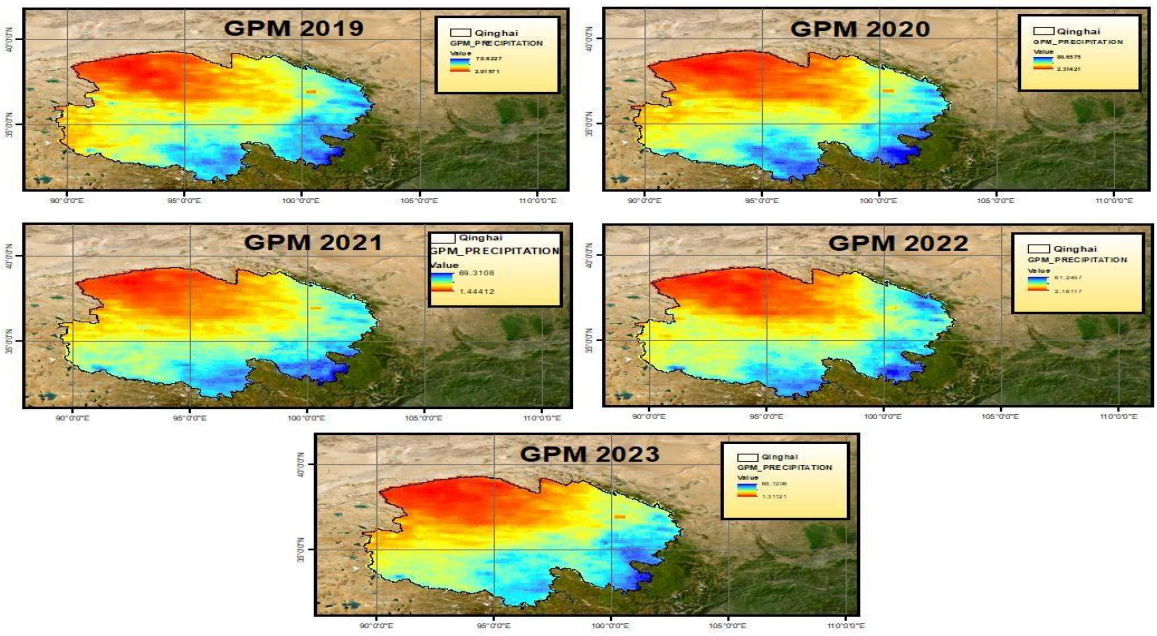

In contrast, the METOP-derived precipitation data (as illustrated in Figure 6) exhibit a more heterogeneous and spatially variable distribution over the same five-year period. Figure 6a presents the contour maps, showing the large-scale precipitation gradients, while Figure 6b displays the detailed spatial distribution patterns, revealing localised variations across Qinghai province. The contour analyses in Figure 6a reveal minimal precipitation variation across most of the study region, with sparse and subtle contour lines indicating relatively uniform low precipitation values throughout Qinghai Province. Unlike the smooth northwest–southeast gradients seen in the GPM data, the METOP contours display limited spatial coherence and weaker regional organisation, reflecting a more fragmented precipitation structure.

The corresponding spatial distribution maps in Figure 6b depict a more complex and irregular pattern, with scattered patches of slightly higher precipitation (shown in yellow/orange) dispersed among predominantly low-precipitation zones (shown in blue/cyan). These fine-scale spatial variations appear intermittently across different years—most notably in 2019, 2021, and 2023—indicating localised precipitation responses captured by the GNSS-RO system. Despite these localised fluctuations, the overall precipitation magnitude remains consistently low across all years, and no systematic regional gradients are observed as in the GPM dataset. This spatial heterogeneity likely reflects both the high vertical sensitivity and limited horizontal sampling density of GNSS-RO measurements, as well as potential artifacts introduced during spatial interpolation and gridding processes.

Figure 6: METOP-based precipitation contours and spatial distribution across Qinghai, China

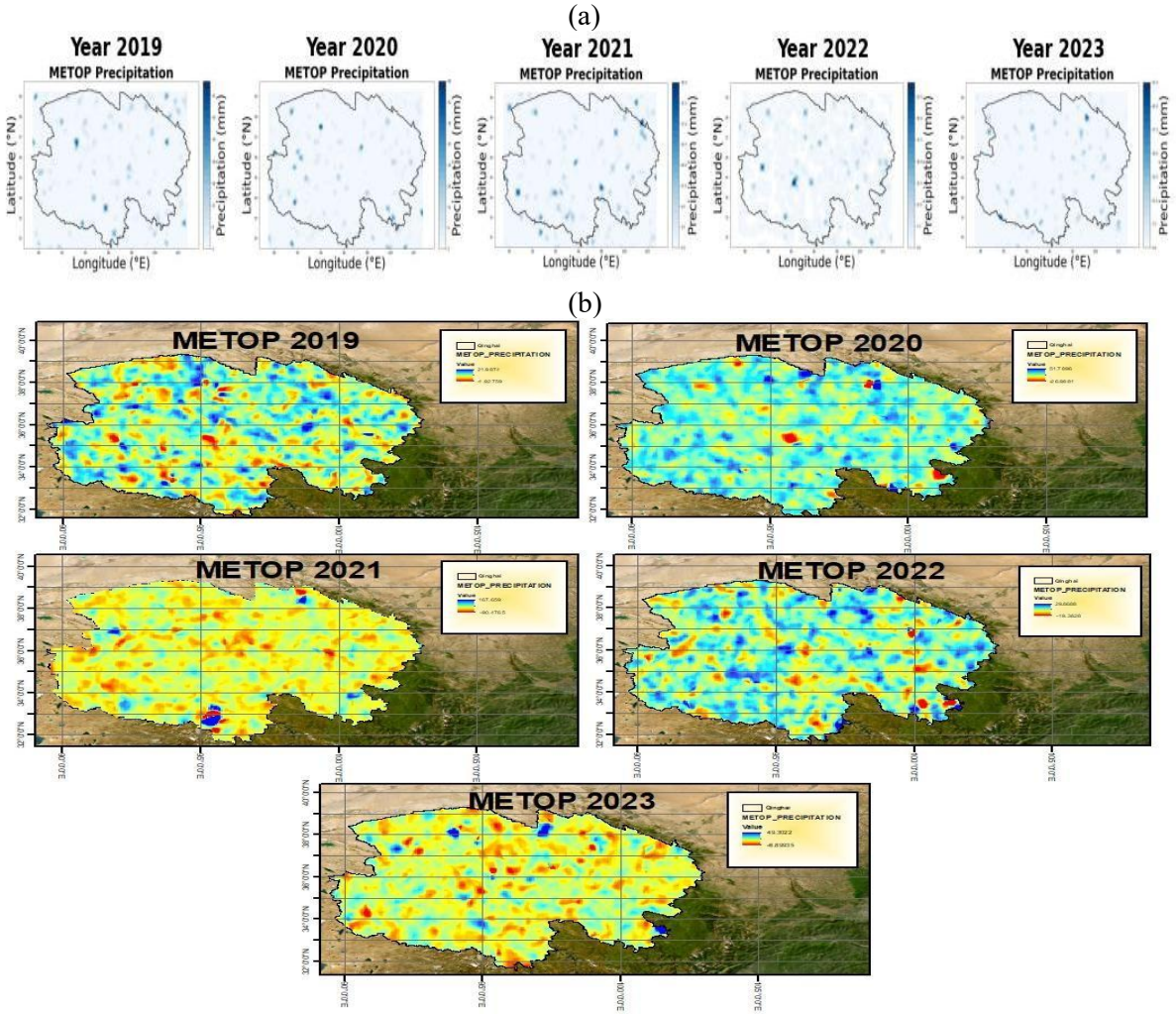

4.2. Air temperature analysis

4.2.1. Statistical performance metrics

Air temperature comparisons between ERA5 (reanalysis) and METOP (GNSS-derived) datasets (as illustrated in Figure 7) reveal notable differences in their mean values and statistical behaviour. Figure 7a presents the ERA5-based performance metrics, while Figure 7b shows the corresponding METOP-derived results, enabling a direct comparison of their error magnitudes and variability. ERA5 exhibited mean air temperatures ranging from 270.65 K to 272.65 K over the study period, whereas METOP consistently produced lower estimates near 263.15 K. This systematic cold deviation in the GNSS-RO–derived temperatures relative to ERA5 likely arises from differences in vertical resolution, retrieval algorithms, and the conversion of atmospheric refractivity to temperature profiles.

Even after bias correction, the metrics shown in Figure 7b indicate that METOP retains higher error values, with MAE and RMSE of around 15–17 °C, suggesting limited accuracy in capturing absolute atmospheric temperatures relative to ERA5. By contrast, Figure 7a shows that ERA5 yields lower RMSE values (approximately 5 °C), indicating tighter agreement with climatological expectations. Overall, the performance statistics in Figure 7 highlight that while GNSS-RO–based temperature retrievals from METOP provide consistent temporal behaviour, their systematic cold bias and broader error spread underscore the need for calibration and regional tuning to improve accuracy over high-altitude regions like Qinghai.

Figure 7: Statistical performance metrics for air temperature data (2019–2023) from ERA5 (top) and METOP (bottom) satellites

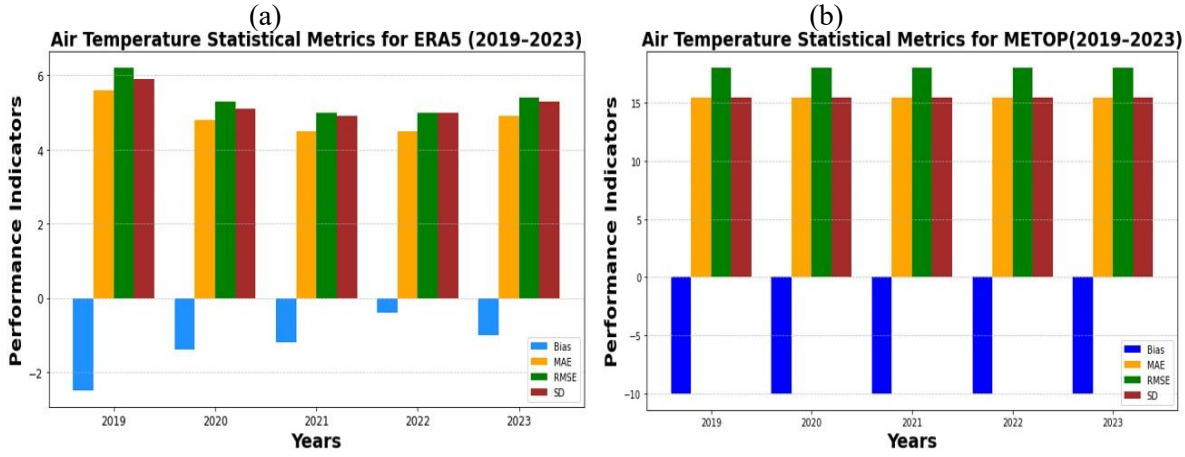

4.2.2. Temporal variations

The yearly average temperature variations (as illustrated in Figure 8) demonstrate distinct temporal trends between the two datasets. Figure 8a displays the ERA5-derived temperature variations, while Figure 8b presents the corresponding METOP (GNSS-RO) results, allowing direct visual comparison of their interannual behaviour. ERA5 shows notable interannual variability, characterized by a warming–cooling–warming pattern across the five-year study period. The highest average temperature occurred in 2019 (276.70 K), followed by a gradual decline to 274.60 K in 2022 and a partial recovery to 275.12 K in 2023, as seen in Figure 8a. This pattern reflects ERA5's sensitivity to annual climatic fluctuations and large-scale atmospheric processes influencing the Qinghai region.

In contrast, Figure 8b shows that METOP-derived temperatures remain remarkably stable throughout 2019–2023, averaging approximately 263.25 K (± 0.1 K). This consistent pattern suggests limited interannual variability, likely resulting from the coarser temporal resolution, vertical averaging, and retrieval constraints inherent to GNSS-RO observations compared to reanalysis data such as ERA5. Overall, Figure 8 underscores the differing sensitivities of the two datasets—ERA5 effectively captures annual temperature fluctuations, while METOP provides stable, bias-free profiles valuable for long-term climate trend monitoring in high-altitude regions.

Figure 8: Yearly average air temperature values (2019–2023) obtained from ERA5 (top) and METOP (bottom) satellites

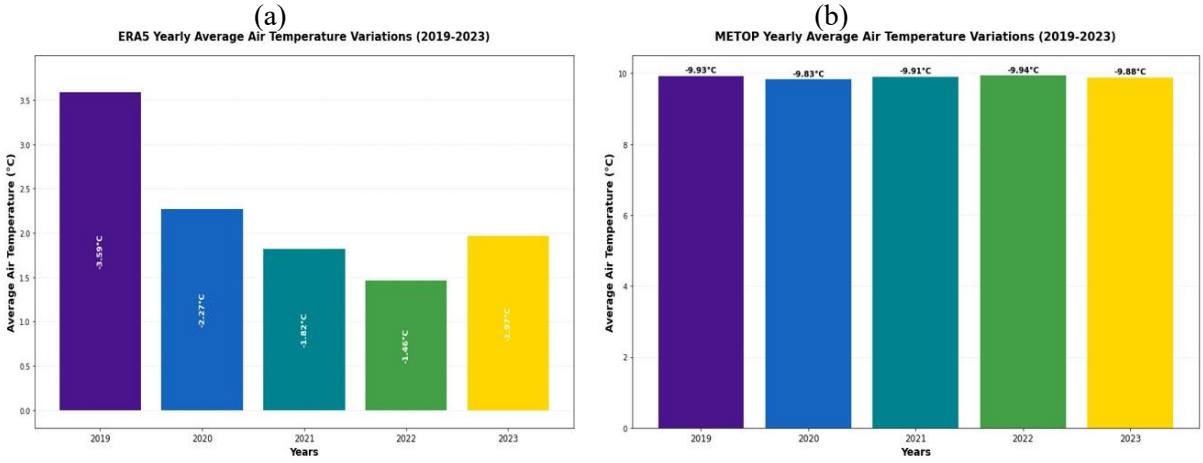

4.2.3. Seasonal variability

The analysis of seasonal air temperature patterns (Figure 9) highlights clear differences in behaviour between the two datasets. Figure 9a illustrates ERA5-derived seasonal temperature variations, while Figure 9b presents the corresponding METOP (GNSS-RO) results, enabling a direct comparison of their temporal characteristics and amplitudes. ERA5 data (Figure 9a) exhibit pronounced seasonal variability, characterised by complex monthly fluctuations that change notably across the five-year period. Peak summer temperatures (June–August) reach approximately 275–278 K, whereas winter minima (December–February) drop to around 265–268 K. The magnitude and pattern of these cycles vary inter-annually, reflecting the dataset's ability to capture short-term climate dynamics and year-to-year atmospheric changes over Qinghai Province.

In contrast, METOP temperature data (Figure 9b) show a much more consistent and predictable seasonal profile throughout 2019–2023. The pattern follows a unimodal cycle, with summer peaks near 268–270 K and winter lows around 255–258 K. Although these values are systematically lower than ERA5, the timing and shape of the seasonal cycle remain stable, indicating reduced inter-annual variation likely due to the GNSS-RO system's coarser temporal resolution and vertical averaging processes. Overall, Figure 9 confirms that both datasets capture the defining continental climate of Qinghai cold winters and relatively warmer summers—**but differ markedly in temperature magnitude. While ERA5 reflects finer temporal variability and higher absolute temperatures, METOP provides smoother and climatologically consistent seasonal signals, reinforcing its potential for long-term climate trend assessment despite underestimation in temperature magnitude.

Figure 9: Yearly average air temperature variations from 2019 to 2023 derived from ERA5 (a) and METOP (b) satellite data

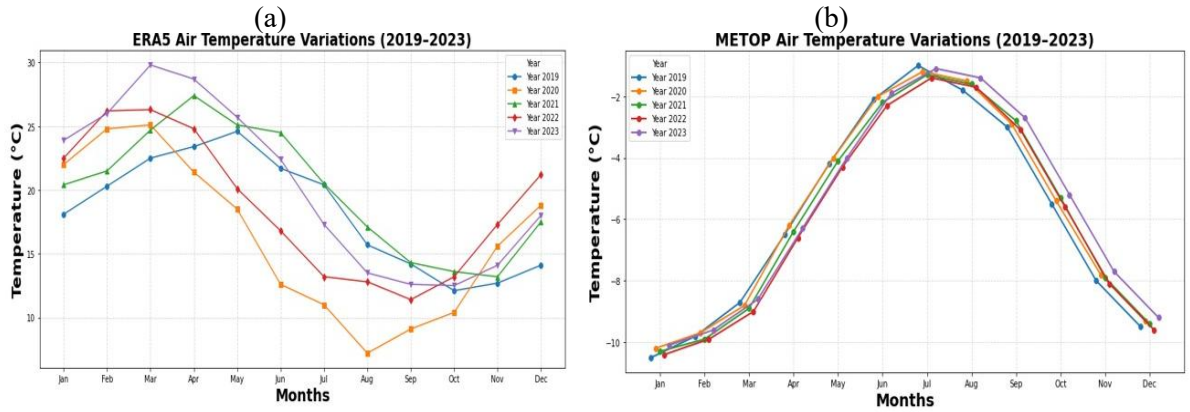

4.2.4. Spatial distribution analysis

The spatial distribution of air temperature across Qinghai province, derived from ERA5 data, shown in Figure 10, reveals a distinct and persistent northwest-to-southeast temperature gradient that remains consistent over the five-year study period. Figure 10a presents the contour maps, which clearly demonstrate this spatial trend—warmer temperatures (in red/orange tones) dominate the northwestern regions, while cooler temperatures (in blue shades) extend toward the southeastern areas. This well-defined pattern remains stable from 2019 to 2023, with contour lines maintaining nearly identical orientations and spacing despite year-to-year variations in overall temperature magnitude, which is observed in the temporal analysis.

The spatial distribution maps, as shown in Figure 10b, provide a more detailed and visually enhanced representation of these temperature gradients. The colour transitions across the province emphasise the gradual decline in temperature from northwest to southeast, consistent with elevation-related and climatic influences typical of Qinghai's topography. The warmer zones are consistently concentrated in the northwestern and central regions, whereas cooler zones persist in the southeast, reinforcing the large-scale spatial coherence detected in ERA5 data. Overall, Figures 10a and 10b collectively confirm that the northwest–southeast temperature gradient is a dominant and recurring spatial feature of the region's climate throughout 2019– 2023. Although absolute temperature values vary slightly across years, the structural stability of the spatial patterns underscores ERA5's robustness in capturing regional temperature distribution and long-term climatic consistency.

Figure 10: Contour and Spatial Maps of ERA5 Air Temperature in Qinghai, China

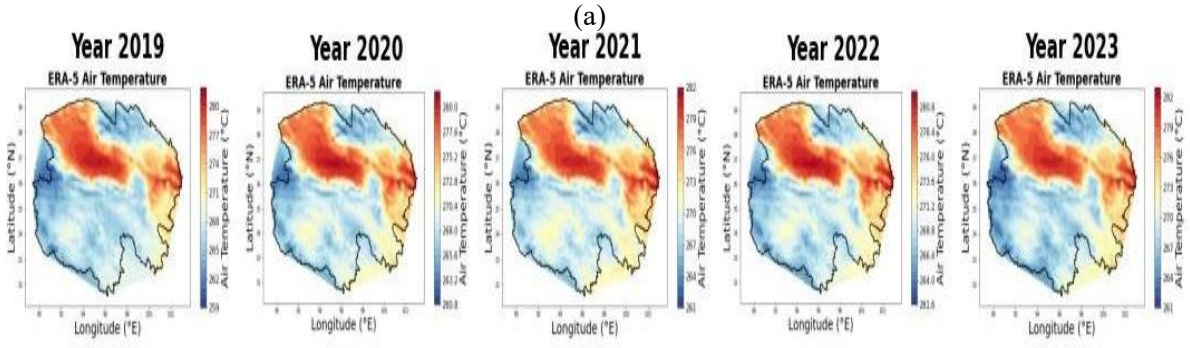

(b)

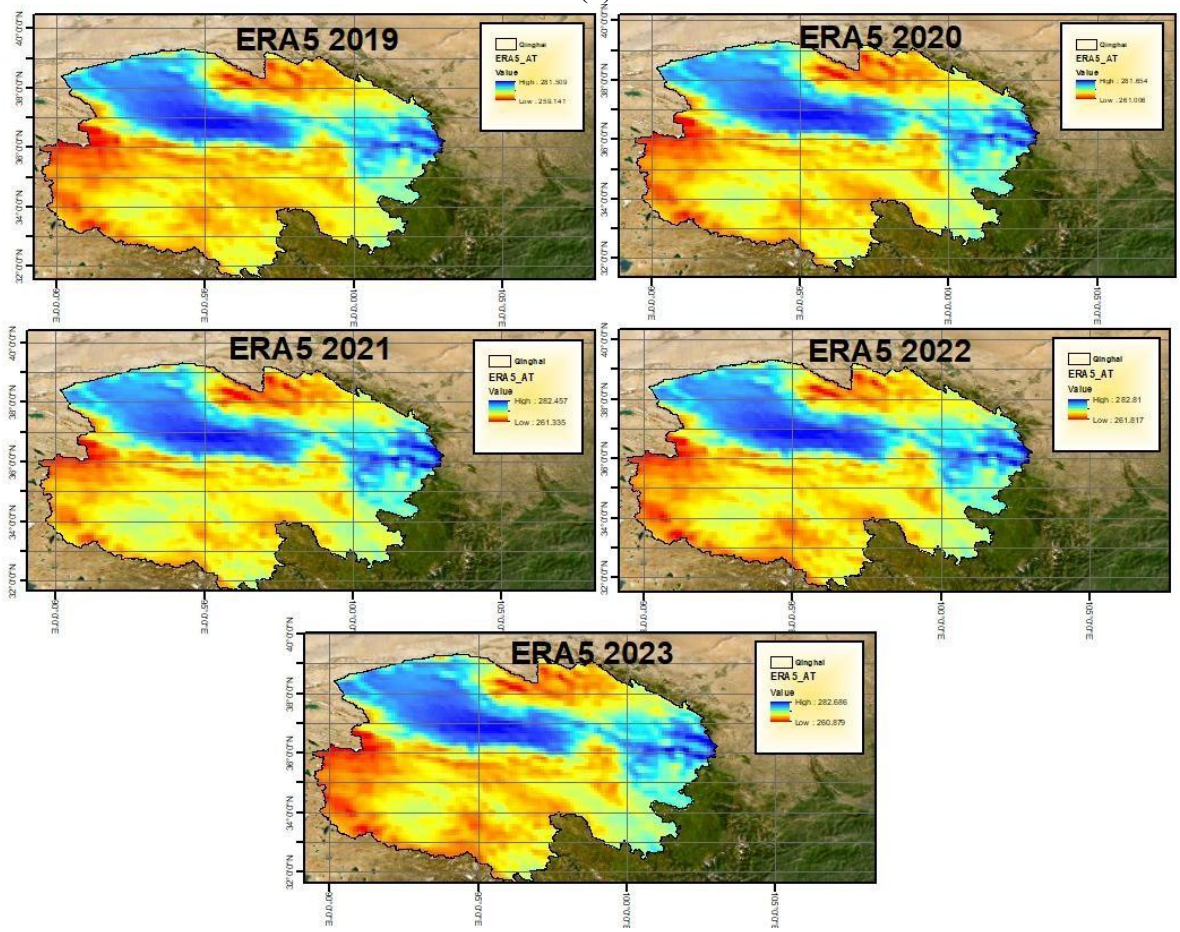

The spatial distribution of air temperature derived from METOP GNSS-RO data presents a more heterogeneous and spatially irregular pattern across Qinghai Province compared to ERA5 (Figure 11). Figure 11a shows the contour maps, where temperature values remain largely uniform across most of the region, consistently within the 262–264 K range. The sparse and subtle contour lines indicate minimal spatial temperature gradients, emphasising the limited spatial variability captured by the GNSS-RO retrievals. Unlike the smooth and structured northwest–southeast temperature gradients observed in the ERA5 dataset, the METOP contours display weak spatial organisation and minimal interannual variation, consistent with the strong temporal stability identified in previous analyses.

The spatial distribution maps (Figure 11b) provide a higher-resolution perspective, illustrating fine-scale temperature fluctuations across the province. These maps reveal scattered patches of slightly higher temperatures (yellow/orange areas) interspersed among predominantly cooler zones (blue/cyan regions). The resulting pixelated texture likely reflects the sparse vertical profile coverage and coarse horizontal interpolation inherent in GNSS-RO temperature retrievals.

Despite the visible heterogeneity, the overall temperature range remains narrow (only about 2–3 K across all years), underscoring the stability of METOP-derived estimates. The absence of a systematic northwest–southeast gradient—clearly evident in the ERA5 maps—suggests that GNSS-RO data are more sensitive to localised atmospheric variability than to broad regional temperature structures. This heterogeneity may arise from GNSS-RO's vertical sensitivity to

refractivity changes at different atmospheric layers, or from limitations in interpolation techniques used for spatial mapping of sparse profile-based observations.

Figure 11: Contour and Spatial Maps of METOP air temperature in Qinghai, China

(a)

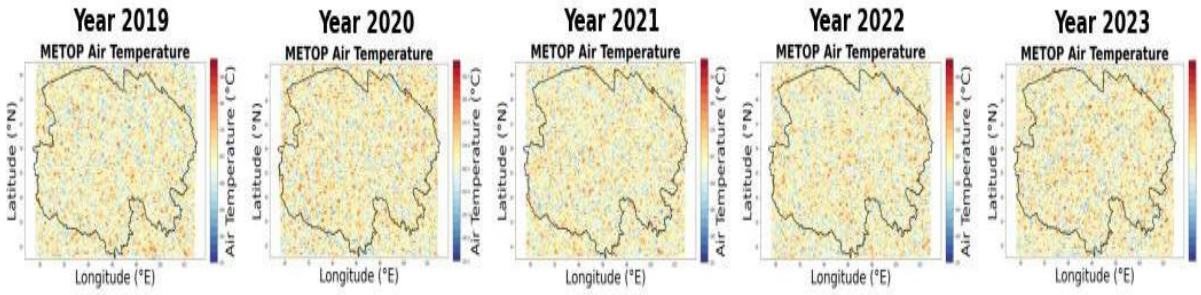

(b)

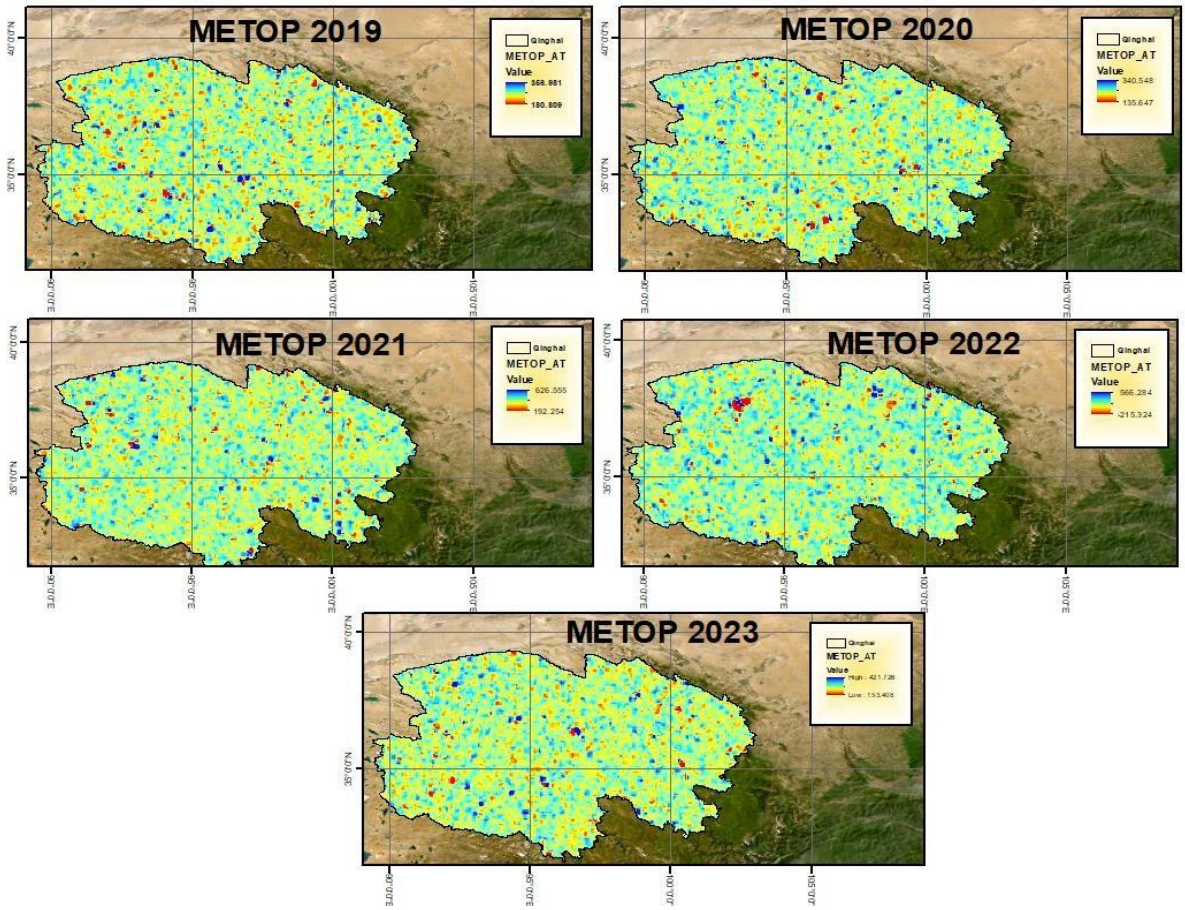

4.3. Evapotranspiration analysis

4.3.1. Statistical performance metrics

The comparison of evapotranspiration (ET) between TerraClimate (model-based) and METOP (GNSS-derived) datasets reveals substantial differences in both magnitude and error metrics (Figure 12). Figure 12a illustrates the TerraClimate-based estimates, which show significantly higher statistical values, with bias and MAE around 2600 mm/year and RMSE exceeding 3000

mm/year. These values appear unusually high for the Qinghai region and may indicate potential overestimation or aggregation artefacts within the model outputs. Such elevated error metrics require further verification to confirm whether they result from actual model behaviour or data processing issues.

In contrast, Figure 12b presents the METOP-derived ET values, which are much lower and more consistent with expected regional evapotranspiration levels. The bias and MAE are approximately 500 mm/year, while the RMSE is around 550 mm/year. Similarly, the unbiased RMSE (UbRMSD) and standard deviation were significantly lower for METOP (~200 mm/year) than for TerraClimate (~1500 mm/year), reinforcing the observation of reduced variability and error in the GNSS-derived dataset.

This contrast highlights a systematic difference in estimation approaches, with the GNSS-derived method yielding more conservative results—likely due to its reliance on atmospheric refractivity rather than modelled land–atmosphere fluxes. The elevated TerraClimate metrics may stem from model parameterisations that tend to overestimate ET in cold, high-altitude regions such as Qinghai, particularly where vegetation and soil characteristics diverge from the model's calibration environments.

Figure 12: Statistical performance metrics for evapotranspiration data (2019–2023) from TerraClimate (top) and METOP (bottom) satellites

(a) (b)

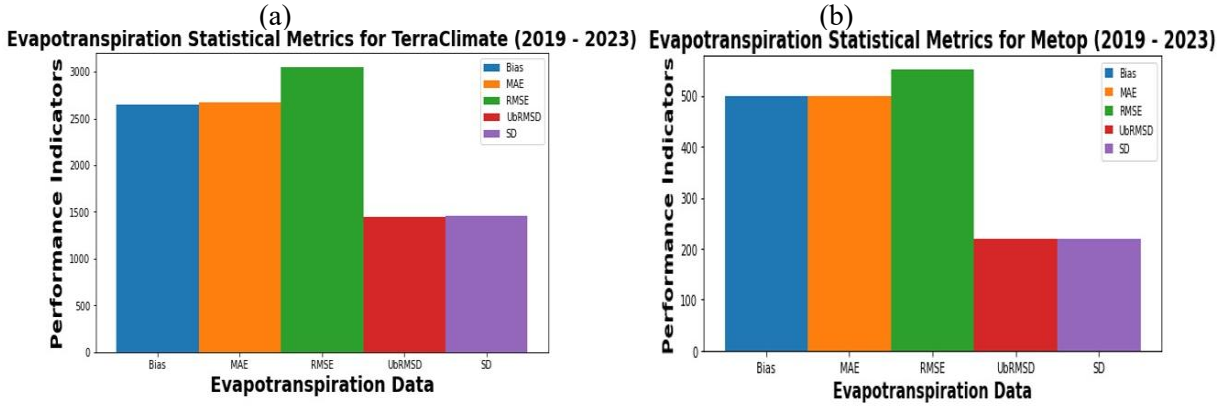

4.3.2. Temporal variations

The comparison of evapotranspiration (ET) between TerraClimate (model-based) and METOP (GNSS-derived) datasets reveal substantial differences in both magnitude and error metrics (Figure 13). Figure 12a illustrates the TerraClimate-based estimates, which show significantly higher statistical values, with bias and MAE around 2600 mm/year and RMSE exceeding 3000 mm/year. These values appear unusually high for the Qinghai region and may indicate potential overestimation or aggregation artefacts within the model outputs. Such elevated error metrics require further verification to confirm whether they result from actual model behaviour or data processing issues.

In contrast, Figure 13b presents the METOP-derived ET values, which are much lower and more consistent with expected regional evapotranspiration levels. The bias and MAE are approximately 500 mm/year, while the RMSE is around 550 mm/year. Similarly, the unbiased RMSE (UbRMSD) and standard deviation were significantly lower for METOP (~200 mm/year) than for TerraClimate (~1500 mm/year), reinforcing the observation of reduced variability and error in the GNSS-derived dataset.

This contrast highlights a systematic difference in estimation approaches, with the GNSS-derived method yielding more conservative results—likely due to its reliance on atmospheric refractivity rather than modelled land–atmosphere fluxes. The elevated TerraClimate metrics may stem from model parameterisations that tend to overestimate ET in cold, high-altitude regions such as Qinghai, particularly where vegetation and soil characteristics diverge from the model's calibration environments.

Figure 13: Yearly average evapotranspiration values (2019–2023) obtained from TerraClimate (top) and METOP (bottom) satellites

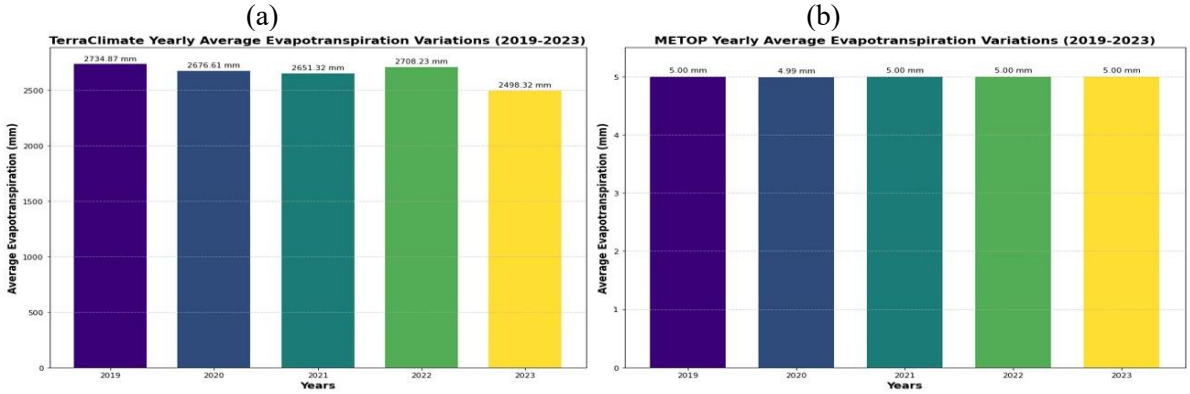

4.3.3. Seasonal analysis

Temporal variations in evapotranspiration exhibit distinct seasonal patterns and interannual differences between the TerraClimate and METOP datasets during the 2019–2023 study period (Figure 14). TerraClimate evapotranspiration exhibits a clear seasonal cycle with peak values during the summer months (June–August), reaching maximum levels around 70–80 mm/month, followed by a gradual decline through autumn and winter months to minimum values near 10–20 mm/month.

The dataset shows year-to-year variations, with different coloured lines representing each year from 2019 to 2023, displaying distinct patterns—particularly during the peak growing season. The winter months (December–February) consistently maintain the lowest evapotranspiration rates across all years, reflecting reduced vegetation activity and limited atmospheric demand during cold periods.

METOP evapotranspiration data reveal a similar seasonal framework but with some differences in magnitude and temporal patterns. The peak evapotranspiration occurs during the same general summer period (June–August), with maximum values reaching approximately 60–70 mm/month, which are generally comparable to TerraClimate values. The METOP dataset shows similar inter-annual variability across the five-year period (2019–2023), displaying different trajectories for each year.

Winter evapotranspiration values remain consistently low in both datasets, typically ranging between 10 and 30 mm/month. Both datasets demonstrate the characteristic seasonal cycle expected for the study region, with the growing season showing elevated evapotranspiration rates and a clear transition to reduced rates during the dormant winter period. This consistent pattern highlights the influence of temperature and vegetation activity on evapotranspiration throughout the year.

Figure 14: Yearly average evapotranspiration variations from 2019 to 2023 derived from TerraClimate (a) and METOP (b) satellite data

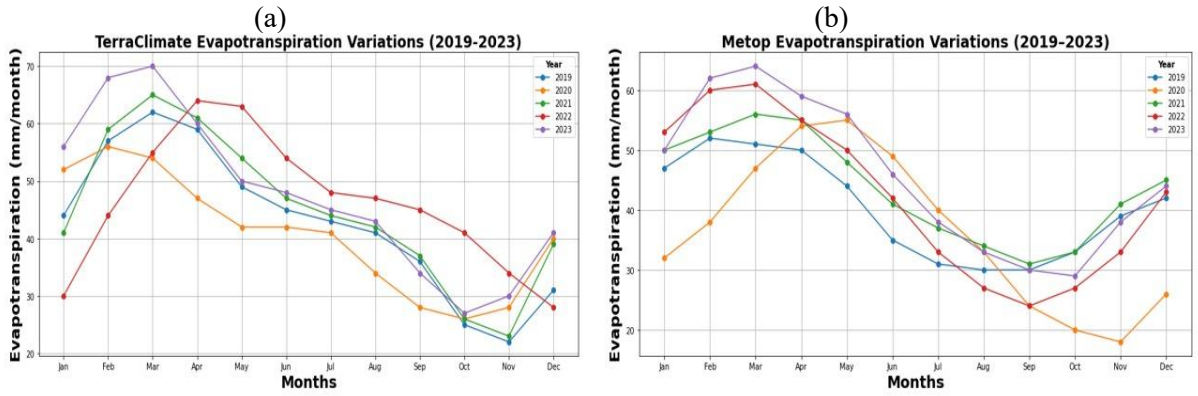

4.3.4. Spatial distribution analysis

The temporal variations in evapotranspiration demonstrate distinct seasonal patterns and interannual differences between TerraClimate and METOP datasets across the 2019–2023 study period (Figure 15). TerraClimate evapotranspiration exhibits a clear seasonal cycle with peak values during the summer months (June–August), reaching maximum levels around 70–80 mm/month, followed by a gradual decline through autumn and winter months to minimum values near 10–20 mm/month.

The dataset shows year-to-year variations, with different coloured lines representing each year from 2019 to 2023, displaying distinct patterns—particularly during the peak growing season. The winter months (December–February) consistently maintain the lowest evapotranspiration rates across all years, reflecting reduced vegetation activity and limited atmospheric demand during cold periods.

METOP evapotranspiration data reveal a similar seasonal framework but with some differences in magnitude and temporal patterns. Peak evapotranspiration occurs during the same general summer period (June–August), with maximum values of approximately 60–70 mm/month, comparable to TerraClimate values. The METOP dataset shows similar interannual variability over the five years (2019–2023), with distinct trajectories for each year.

Winter evapotranspiration values remain consistently low across both datasets, typically ranging from 10 to 30 mm/month. Both datasets demonstrate the characteristic seasonal cycle expected for the study region, with the growing season showing elevated evapotranspiration rates and a clear transition to reduced rates during the dormant winter period.

Figure 15: Contour and spatial maps of terraClimate evapotranspiration in Qinghai, China

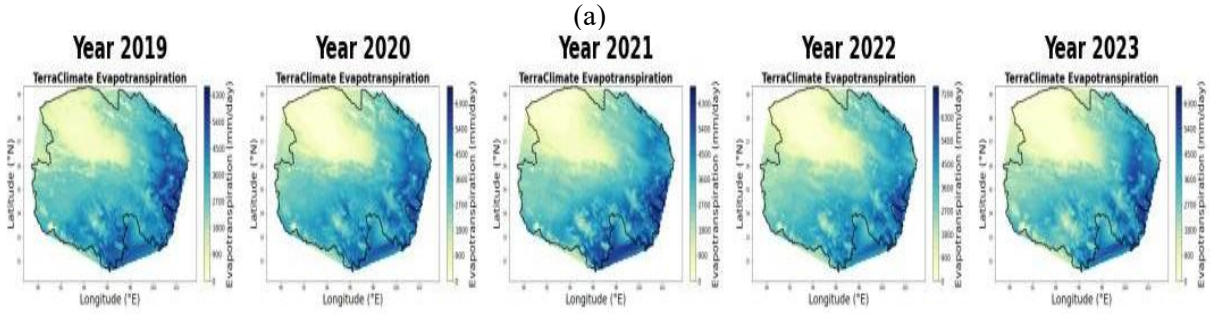

(b)

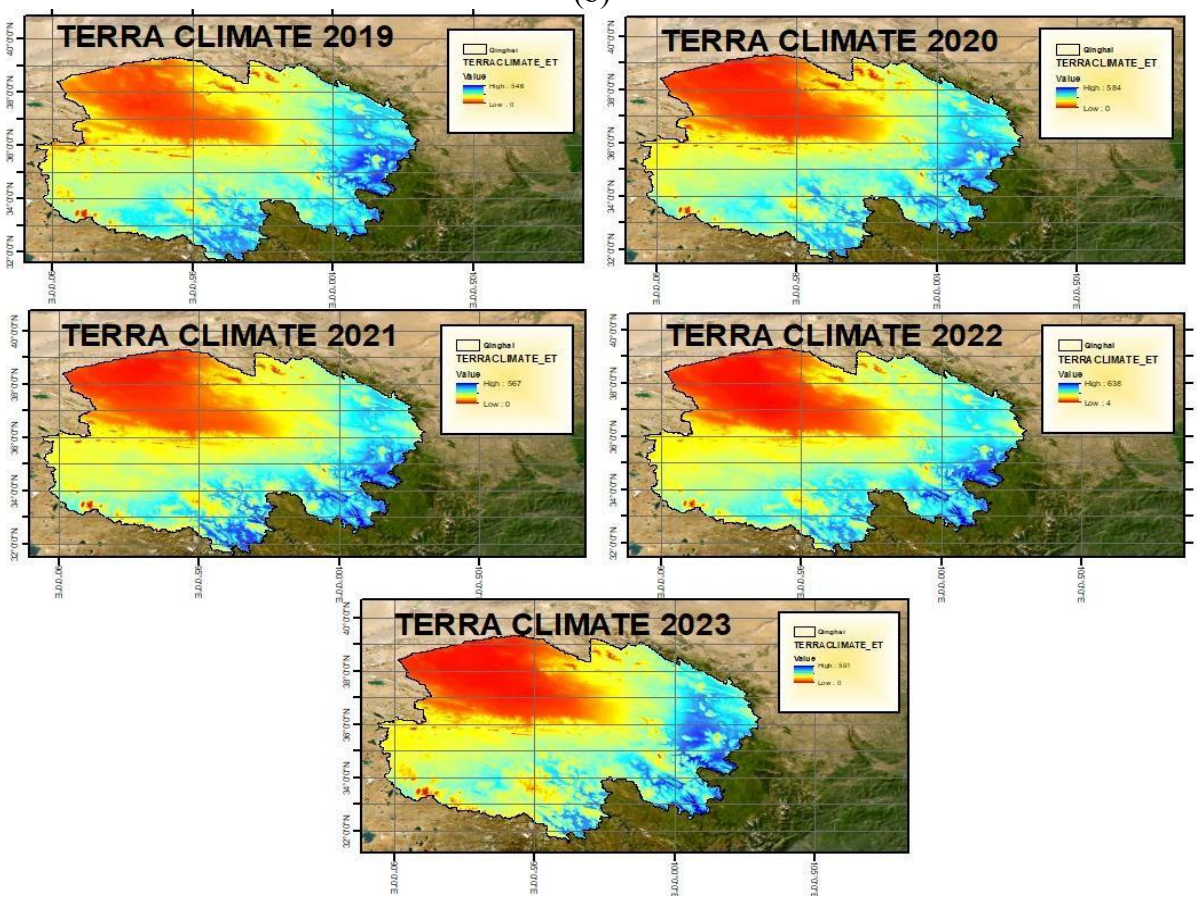

The METOP-derived evapotranspiration (ET) maps across Qinghai Province from 2019 to 2023 (Figure 16a and b) exhibit spatial patterns that appear broadly uniform at the regional scale but contain localised variability at finer resolutions. The contour plots show persistently low ET values across most of the province, with minimal large-scale spatial gradients and subtle interannual changes—suggesting low regional sensitivity to topographic or climatic variation. In contrast, the gridded spatial distribution maps reveal localised patches of slightly elevated ET (depicted in yellow/orange) embedded within widespread low-ET zones (blue/cyan), forming a pixelated, mosaic-like pattern. This fine-scale heterogeneity remains relatively consistent throughout the study period, although the overall magnitude of ET stays within a narrow range (typically around 500 mm/year with minor fluctuations). The observed spatial noise may reflect both the limited spatial resolution and sampling density of GNSS radio occultation data, as well as potential artefacts introduced during interpolation from sparse atmospheric profiles in this high-altitude, arid region.

Figure 16: Contour and spatial maps of METOP evapotranspiration in Qinghai, China

(a)

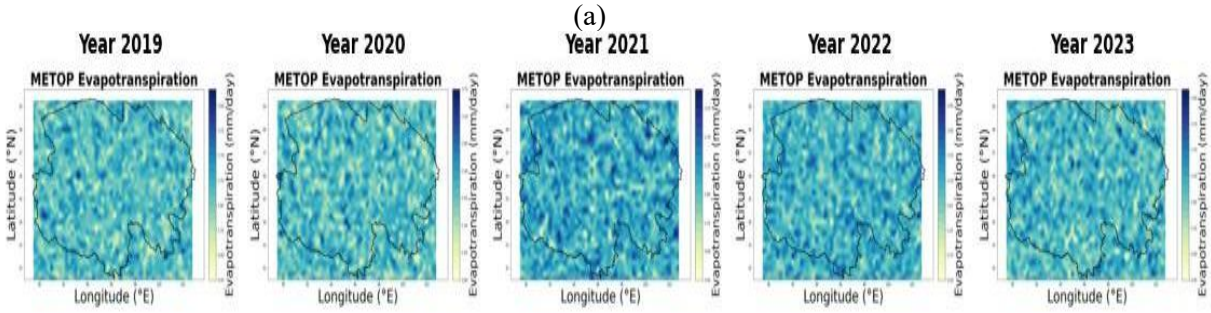

(b)

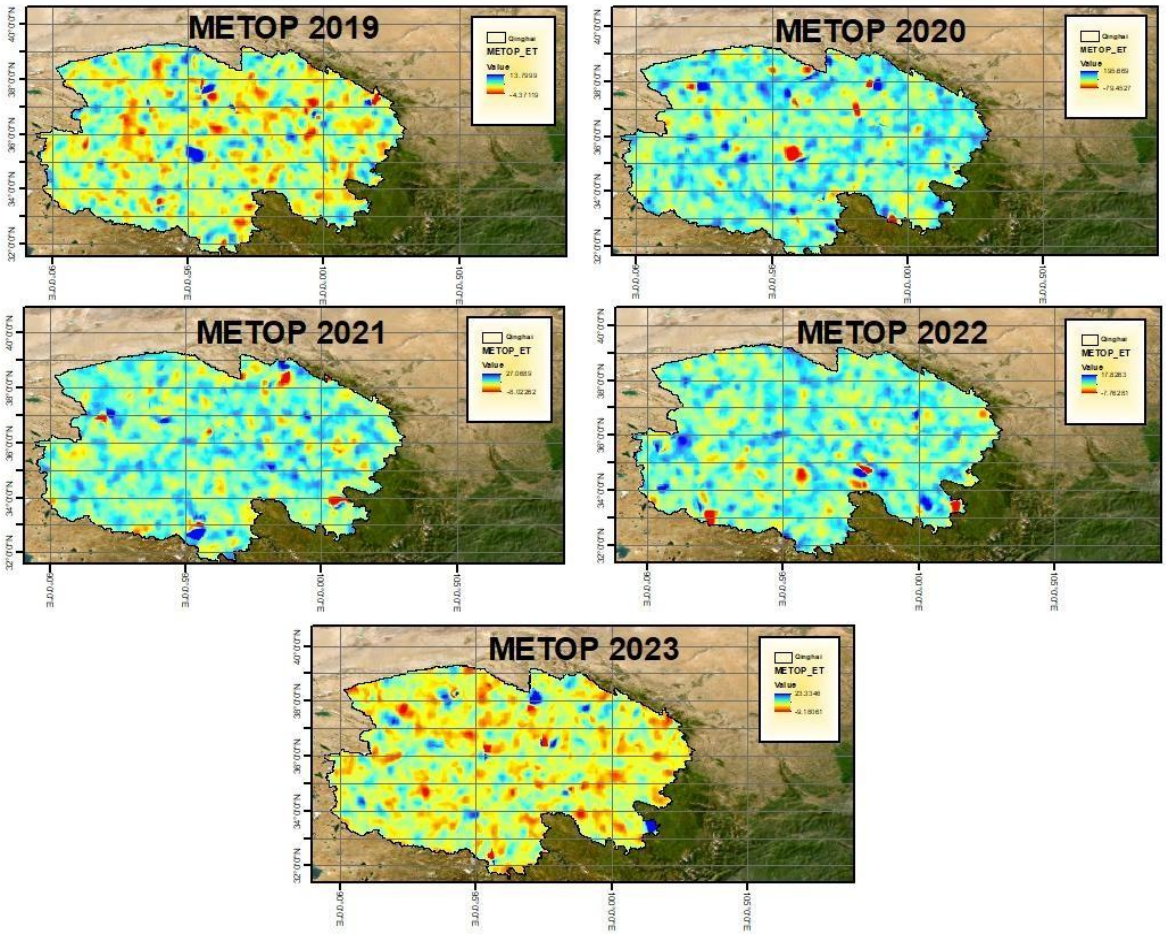

5. Discussion and analysis

This study conducted a comprehensive comparison between GNSS Radio Occultation (RO) derived climate variables from the METOP satellite and conventional remote sensing and reanalysis datasets, specifically GPM for precipitation, ERA5 for air temperature, and TerraClimate for evapotranspiration across Qinghai Province, China, during 2019–2023. The objective was to assess the performance, stability, and spatiotemporal characteristics of GNSS-derived climate estimates relative to established climate datasets. Across all three climate variables, METOP-derived values consistently exhibited lower magnitudes and greater temporal stability than their conventional counterparts. The METOP GNSS RO precipitation estimates demonstrated substantially lower bias (≈ 2.1 mm) and RMSE (≈ 5.9 mm) compared to GPM (bias ≈ 18.6 mm; RMSE ≈ 22.7 mm), indicating superior accuracy in GNSS-derived precipitation. This aligns with findings by (He *et al.*, 2017), who reported GPM's tendency to overestimate precipitation in complex terrain. Similarly, (Shehaj *et al.*, 2025) highlighted the long-term stability and all-weather retrieval capability of GNSS RO products, although previous studies have seldom focused on high-altitude regions such as Qinghai, a gap directly addressed in this work.

Persistent retrieval limitations in GPM, particularly signal attenuation and surface contamination in high-altitude regions, have been noted in comprehensive evaluation studies over the Qinghai Tibet Plateau. Dahri *et al.* (2021) likewise reported degraded performance of gridded precipitation products across steep topography and monsoon-influenced zones. Our

spatial analysis supports these conclusions, as METOP captured fine-scale precipitation hotspots shaped by local topography, an effect suspected by (Ren *et al.*, 2024) but unresolved in coarse-resolution datasets. Temporally, METOP precipitation exhibited minimal interannual variability (~ ± 0.01 mm), whereas GPM showed fluctuations of up to 43%, underscoring the superior stability of GNSS RO data for long-term climatic monitoring in mountainous regions consistent with evaluation studies across the QTP.

Regarding temperature, GNSS RO provided vertically resolved profiles capable of detecting tropospheric warming and stratospheric cooling. (Heise *et al.*, 2006) demonstrated GNSS RO's value for tropospheric water vapour monitoring aboard CHAMP, while (Wu *et al.*, 2024) emphasised the importance of ionospheric error correction for accurate temperature retrievals, a consideration incorporated into our processing pipeline to minimise bias. METOP-derived temperature values were systematically cooler (~ 263 K) than ERA5 (~ 270–273 K), exhibiting limited interannual variability and suggesting higher measurement stability. These differences likely reflect methodological divergences, including distinct vertical resolutions, retrieval assumptions, and sensitivities to surface and atmospheric conditions. Evapotranspiration (ET) analyses revealed pronounced divergence between datasets. TerraClimate exhibited a notable decline from 2735 mm (2019) to 2498 mm (2023), with a statistically significant negative trend (slope = −59.14 mm yr^{-1}, $p = 0.02$), a finding consistent with (Meng *et al.*, 2024), who linked declining ET trends to reduced vegetation cover and altered precipitation regimes. However, these prior studies relied primarily on model-based estimates lacking vertical validation.

In contrast, METOP GNSS RO–derived ET remained nearly constant (~ 5.00 mm ± 0.01 mm), reflecting GNSS RO's atmospheric sensitivity and relative insensitivity to land surface flux variations, as also noted by (Vaquero-Martínez & Antón, 2021). This stability supports the interpretation that GNSS RO data capture large-scale atmospheric consistency rather than surface-driven hydrological fluctuations. Our findings emphasise that previous research often advocated multi-source integration but rarely conducted detailed intercomparisons between vertical (GNSS RO) and surface-based (RS/reanalysis) datasets within consistent spatial and temporal domains. This study addresses this limitation by explicitly comparing both retrieval modes across identical variables, terrain, and periods (2019–2023) over Qinghai province. The integrated approach yields nuanced insights: GNSS RO excels in vertical precision, retrieval robustness, and immunity to cloud cover, whereas remote sensing products capture surface-driven processes such as precipitation extremes and evapotranspiration variability.

The observed discrepancies, such as the overestimation of ET and precipitation in surface-based datasets and the high vertical stability of GNSS RO, underscore the importance of data fusion. (Mingyue *et al.*, 2019) reported that long-term spatial and temporal ET variability across the Qinghai Tibet Plateau is largely driven by temperature increases and precipitation redistribution, while (Liu *et al.*, 2021) demonstrated that multi-source data integration, particularly incorporating vegetation and land surface information, is essential for resolving local-scale ET dynamics. These perspectives align with our conclusion that GNSS RO offers vertically resolved, bias-resistant atmospheric observations, whereas conventional remote sensing provides valuable insight into surface processes.

6. Conclusions

Overall, the results establish GNSS RO, particularly METOP, as a stable, high-fidelity observational framework suited for monitoring long-term climate variability in

topographically complex, data-sparse regions such as Qinghai Province. While GNSS RO data lack the temporal responsiveness and spatial smoothness of traditional datasets, their exceptional vertical resolution, consistency, and independence from land-surface effects make them uniquely valuable for climate model calibration and regional bias correction. Future work should focus on (i) calibration with ground-based or well-validated satellite products, (ii) enhanced interpolation and gridding techniques for sparse GNSS RO profiles, (iii) region-specific retrieval tuning for cold, high-elevation environments, and (iv) integration of machine learning methods to improve temporal sensitivity and pattern recognition. Collectively, these efforts will unlock the full potential of GNSS-based climate monitoring systems, enabling a synergistic fusion of atmospheric and surface datasets for more reliable detection of climate trends across the Qinghai–Tibet Plateau and other high-altitude regions.

Declaration of conflict of interest:

The author(s) declared no potential conflicts of interest(s) with respect to the research, authorship, and/or publication of this article.

Funding:

The author(s) received no financial support for the research, authorship and/or publication of this article.

Publisher's Note:

IDEA Publishers Group (NASIJ IDEA-PG) stands neutral with regard to jurisdictional claims in the published maps and institutional affiliations.

References

Abatzoglou, J., Parks, S. D. S., & Hegewisch, K. (2017). Data Descriptor: TerraClimate, a high resolution global dataset of monthly climate and climatic water balance from 1958-2015. *Scientific Data, 5*, 170191. https://doi.org/10.1038/sdata.2017.191

Ajjur, S. B., & Al-Ghamdi, S. G. (2021). Evapotranspiration and water availability response to climate change in the Middle East and North Africa. *Climatic Change*, *166*(3), 28. https://doi.org/10.1007/s10584-021-03122-z

An, H., Song, X., Wang, Z., Geng, X., Zhou, P., Zhai, J., & Sun, W. (2024). Investigating the longterm response of plateau vegetation productivity to extreme climate: insights from a case study in Qinghai Province, China. *International Journal of Biometeorology*, *68*(2), 333349. https://doi.org/10.1007/s00484-023-02593-2

Anthes, R. A., Bernhardt, P., Chen, Y., Cucurull, L., Dymond, K., Ector, D., Healy, S., Ho, S.-P., Hunt, D., & Kuo, Y.-H. (2008). The COSMIC/FORMOSAT-3 mission: Early results. *Bulletin of the American Meteorological Society*, *89*(3), 313–334. https://doi.org/10.1175/BAMS-89-3-313

Araghi, A., Martinez, C. J., & Adamowski, J. F. (2023). Evaluation of TerraClimate gridded data across diverse climates in Iran. *Earth Science Informatics*, *16*(2), 1347–1358. https://doi.org/10.1007/s12145-023-00967-z

Clerbaux, C., Boynard, A., Clarisse, L., George, M., Hadji-Lazaro, J., Herbin, H., Hurtmans, D., Pommier, M., Razavi, A., & Turquety, S. (2009). Monitoring of atmospheric composition using the thermal infrared IASI/MetOp sounder. *Atmospheric Chemistry and Physics*, *9*(16), 6041–6054. https://doi.org/10.5194/acp-9-6041-2009

Cracknell, A. P., & Varotsos, C. A. (2011). New aspects of global climate-dynamics research and remote sensing. *International Journal of Remote Sensing*, *32*(3), 579–600. https://doi.org/10.1080/01431161.2010.517807

Dahri, Z. H., Ludwig, F., Moors, E., Ahmad, S., Ahmad, B., Shoaib, M., Ali, I., Iqbal, M. S., Pomee, M. S., & Mangrio, A. G. (2021). Spatio-temporal evaluation of gridded precipitation products for the high-altitude Indus basin. *International Journal of Climatology*, *41*(8), 4283-4306. https://doi.org/10.1002/joc.7073

Ding, T., Awange, J. L., Scherllin-Pirscher, B., Kuhn, M., Khandu, Anyah, R., Zerihun, A., & Bui, L. K. (2022). GNSS radio occultation infilling of the African radiosonde data gaps reveals drivers of tropopause climate variability. *Journal of Geophysical Research: Atmospheres*, *127*(17), e2022JD036648. https://doi.org/10.1029/2022JD036648

Draper, D. W., Newell, D. A., Wentz, F. J., Krimchansky, S., & Skofronick-Jackson, G. M. (2015). The global precipitation measurement (GPM) microwave imager (GMI): Instrument overview and early on-orbit performance. *IEEE Journal of Selected Topics in Applied Earth Observations and Remote Sensing*, *8*(7), 3452–3462. https://doi.org/10.1109/JSTARS.2015.2403303

Gleisner, H., Ringer, M. A., & Healy, S. B. (2022). Monitoring global climate change using GNSS radio occultation. *Npj Climate and Atmospheric Science*, *5*(1), 6. https://doi.org/10.1038/s41612-022-00229-7

Hanchane, M., Kessabi, R., Krakauer, N. Y., Sadiki, A., El Kassioui, J., & Aboubi, I. (2023). Performance Evaluation of TerraClimate Monthly Rainfall Data after Bias Correction in the Fes-Meknes Region (Morocco). *Climate*, *11*(6), 120. https://doi.org/10.3390/cli11060120

Hassan, S. U., Shah, M., Shahzad, R., Ghaffar, B., Li, B., de Oliveira-Júnior, J. F., Vafaeva, K. M., & Jamjareegulgarn, P. (2024). Performance of multi-source remote sensing soil moisture products over Punjab Pakistan during 2022–2023. *Theoretical and Applied Climatology*, *155*(8), 7499–7513. https://doi.org/10.1007/s00704-024-05082-7

He, Z., Yang, L., Tian, F., Ni, G., Hou, A., & Lu, H. (2017). Intercomparisons of rainfall estimates from TRMM and GPM multisatellite products over the Upper Mekong River Basin. *Journal of Hydrometeorology*, *18*(2), 413-430. https://doi.org/10.1175/JHM-D-16-0198.1

Heise, S., Wickert, J., Beyerle, G., Schmidt, T., & Reigber, C. (2006). Global monitoring of tropospheric water vapor with GPS radio occultation aboard CHAMP. *Advances in Space Research*, *37*(12), 2222-2227. https://doi.org/10.1016/j.asr.2005.06.066

Jin, S., & Komjathy, A. (2010). GNSS reflectometry and remote sensing: New objectives and results. *Advances in Space Research*, *46*(2), 111–117. https://doi.org/10.1016/j.asr.2010.01.014

Kazemi Garajeh, M., Haji, F., Tohidfar, M., Sadeqi, A., Ahmadi, R., & Kariminejad, N. (2024). Spatiotemporal monitoring of climate change impacts on water resources using an integrated approach of remote sensing and Google Earth Engine. *Scientific reports*, *14*(1), 5469. https://doi.org/10.1038/s41598-024-56160-9

Ke, C.-Q., Yu, T., Yu, K., Tang, G.-D., & King, L. (2009). Snowfall trends and variability in Qinghai, China. *Theoretical and Applied Climatology*, *98*, 251–258. https://doi.org/10.1007/s00704-009-0105-1

Kursinski, E., & Hajj, G. (2001). A comparison of water vapor derived from GPS occultations and global weather analyses. *Journal of Geophysical Research: Atmospheres*, *106*(D1), 1113–1138. https://doi.org/10.1029/2000JD900421

Kursinski, E., Hajj, G., Schofield, J., Linfield, R., & Hardy, K. R. (1997). Observing Earth's atmosphere with radio occultation measurements using the Global Positioning System. *Journal of Geophysical Research: Atmospheres*, *102*(D19), 23429–23465. https://doi.org/10.1029/97JD01569

Liu, J., Zhou, Y., Lu, F., Yu, Y., Yan, D., Hu, Y., & Xue, W. (2023). Evaluating satellite-and reanalysis-based precipitation products over the Qinghai-Tibetan Plateau in the perspective of a new error-index system. *International Journal of Climatology*, *43*(5), 2200–2219. https://doi.org/10.1002/joc.7970

Liu, Y., Yue, Q., Wang, Q., Yu, J., Zheng, Y., Yao, X., & Xu, S. (2021). A framework for actual evapotranspiration assessment and projection based on meteorological, vegetation and hydrological remote sensing products. *Remote Sensing*, *13*(18), 3643. https://doi.org/10.3390/rs13183643

Meng, S., Tang, Z., Xue, Y., Wu, X., Li, C., & Wu, X. (2024). Relationship between Area Changes of Key Lakes and Evapotranspiration in Qinghai Province. *Atmosphere*, *15*(10), 1210. https://doi.org/10.3390/atmos15101210

Mingyue, C., Junbang, W., Shaoqiang, W., Hao, Y., & Yingnian, L. (2019). Temporal and spatial distribution of evapotranspiration and its influencing factors on Qinghai-Tibet Plateau from 1982 to 2014. *Journal of Resources and Ecology*, *10*(2), 213–224. https://doi.org/10.5814/j.issn.1674-764x.2019.02.012

Moses, M., Ibrahim, U., & Akomolafe, E. (2023). Evaluation of GNSS Radio Occultation Technology for Meteorological and Climate Applications over Nigeria. *Evaluation*, *7*(3), 461–484. https://doi.org/10.36263/nijest.2023.03.04

Newell, D., Draper, D., Remund, Q., Figgins, D., Krimchansky, S., Wentz, F., & Meissner, T. (2015). GPM microwave imager (GMI) on-orbit performance and calibration results. *IEEE International Geoscience and Remote Sensing Symposium (IGARSS)*. https://doi.org/10.1109/IGARSS.2015.7326995

Peng, J., Loew, A., Chen, X., Ma, Y., & Su, Z. (2016). Comparison of satellite-based evapotranspiration estimates over the Tibetan Plateau. *Hydrology and Earth System Sciences*, *20*(8), 3167–3182. https://doi.org/10.5194/hess-20-3167-2016

Ren, Z., Sang, Y. F., Cui, P., Chen, D., Zhang, Y., Gong, T., Sun, S., & Mellouli, N. (2024). Temporal scaling characteristics of sub-daily precipitation in Qinghai-Tibet Plateau. *Earth's Future*, *12*(3), e2024EF004417. https://doi.org/10.1029/2024EF004417

Sa'i, I. U., Aleem, K., Musa, T. A., Youngu, T. T., Obadaki, Y., Anom, W. A., & Nasara, M. A. (2024). An investigation of GNSS RO data pattern for climate change monitoring and analysis over Africa. https://doi.org/10.21203/rs.3.rs-4422572/v1

Shehaj, E., Leroy, S., Cahoy, K., Geiger, A., Crocetti, L., Moeller, G., Soja, B., & Rothacher, M. (2025). Global Navigation Satellite System (GNSS) radio occultation climatologies mapped by machine learning and Bayesian interpolation. *Atmospheric Measurement Techniques*, *18*(1), 57-72. https://doi.org/10.5194/amt-18-57-2025

Skofronick-Jackson, G., Kirschbaum, D., Petersen, W., Huffman, G., Kidd, C., Stocker, E., & Kakar, R. (2018). The Global Precipitation Measurement (GPM) mission's scientific achievements and societal contributions: Reviewing four years of advanced rain and snow observations. *Quarterly Journal of the Royal Meteorological Society*, *144*, 27–48. https://doi.org/10.1002/qj.3313

Steiner, A., Hunt, D., Ho, S.-P., Kirchengast, G., Mannucci, A., Scherllin-Pirscher, B., Gleisner, H., Von Engeln, A., Schmidt, T., & Ao, C. (2013). Quantification of structural

uncertainty in climate data records from GPS radio occultation. *Atmospheric Chemistry and Physics*, *13*(3), 1469–1484. https://doi.org/10.5194/acp-13-1469-2013

Steiner, A. K., Ladstädter, F., Ao, C. O., Gleisner, H., Ho, S.-P., Hunt, D., Schmidt, T., Foelsche, U., Kirchengast, G., & Kuo, Y.-H. (2020). Consistency and structural uncertainty of multimission GPS radio occultation records. *Atmospheric Measurement Techniques*, *13*(5), 2547–2575. https://doi.org/10.5194/amt-13-2547-2020

Sun, T., Yang, Y. M., Wang, Z. G., Yong, Z. W., Xiong, J. N., Ma, G. L., Li, J., & Liu, A. (2023). Spatiotemporal variation of ecological environment quality and extreme climate drivers on the Qinghai-Tibetan Plateau. *Journal of Mountain Science*, *20*(8), 2282–2297. https://doi.org/10.1007/s11629-023-8025-6

Tran, B. N., Van Der Kwast, J., Seyoum, S., Uijlenhoet, R., Jewitt, G., & Mul, M. (2023). Uncertainty assessment of satellite remote-sensing-based evapotranspiration estimates: a systematic review of methods and gaps. *Hydrology and Earth System Sciences*, *27*(24), 4505–4528. https://doi.org/10.5194/hess-27-4505-2023

Trenberth, K. E. (2011). Changes in precipitation with climate change. *Climate research*, *47*(1-2), 123–138. https://doi.org/10.3354/cr00953

Trent, T., Siddans, R., Kerridge, B., Schröder, M., Scott, N. A., & Remedios, J. (2023). Evaluation of tropospheric water vapour and temperature profiles retrieved from MetOp-A by the Infrared and Microwave Sounding scheme. *Atmospheric Measurement Techniques*, *16*(6), 1503–1526. https://doi.org/10.5194/amt-16-1503-2023

Vannah, S., Leroy, S. S., Ao, C. O., Kursinski, E. R., Nelson, K. J., Wang, K.-N., & Xie, F. (2025). The impact of differences in retrieval algorithms between processing centers on GNSS radio occultation refractivity retrievals in the planetary boundary layer. *Atmospheric Measurement Techniques*, *18*(17), 4293–4310. https://doi.org/10.5194/amt-18-4293-2025

Vaquero-Martínez, J., & Antón, M. (2021). Review on the role of GNSS meteorology in monitoring water vapor for atmospheric physics. *Remote Sensing*, *13*(12), 2287. https://doi.org/10.3390/rs13122287

Wang, X. (2023). Remote sensing applications to climate change. *Remote Sensing*, *15*(3), 747. https://doi.org/10.3390/rs15030747

Wu, D. L., Yudin, V. A., Kim, K.-M., Chattopadhyay, M., Coy, L., Lieberman, R. S., Salinas, C. J. H., Lee, J. H., Gong, J., & Liu, G. (2024). GNSS-RO residual ionospheric error (RIE): a new method and assessment. *Atmospheric Measurement Techniques Discussions*, *2024*, 139. https://doi.org/10.5194/amt-18-843-2025

Wu, D. L., Yudin, V. A., Kim, K.-M., Chattopadhyay, M., Coy, L., Lieberman, R. S., Salinas, C. J. H., Lee, J. H., Gong, J., & Liu, G. (2024). GNSS-RO residual ionospheric error (RIE): a new method and assessment. *Atmospheric Measurement Techniques Discussions*, *2024*, 1–39. https://doi.org/10.5194/amt-18-843-2025

Wulfmeyer, V., Hardesty, R. M., Turner, D. D., Behrendt, A., Cadeddu, M. P., Di Girolamo, P., Schlüssel, P., Van Baelen, J., & Zus, F. (2015). A review of the remote sensing of lower tropospheric thermodynamic profiles and its indispensable role for the understanding and the simulation of water and energy cycles. *Reviews of Geophysics*, *53*(3), 819–895. https://doi.org/10.1002/2014RG000476

Yang, J., Gong, P., Fu, R., Zhang, M., Chen, J., Liang, S., Xu, B., Shi, J., & Dickinson, R. (2013). The role of satellite remote sensing in climate change studies. *Nature climate change*, *3*(10), 875–883. https://doi.org/10.1038/nclimate1908

Yang, K., Wu, H., Qin, J., Lin, C., Tang, W., & Chen, Y. (2014). Recent climate changes over the Tibetan Plateau and their impacts on energy and water cycle: A review. *Global and Planetary Change*, *112*, 79–91. https://doi.org/10.1016/j.gloplacha.2013.12.001

Yu, K., Rizos, C., Burrage, D., Dempster, A. G., Zhang, K., & Markgraf, M. (2014). An overview of GNSS remote sensing. *EURASIP Journal on Advances in Signal Processing*, *2014*(1), 134. https://doi.org/10.1186/1687-6180-2014-134

Zhang, S., Liu, F., Li, H., Zhou, Q., Chen, Q., Ma, W., Luo, J., & Huang, Y. (2023). Global Navigation Satellite System-Based Retrieval of Precipitable Water Vapor and Its Relationship with Rainfall and Drought in Qinghai, China. *Atmosphere*, *14*(3), 517. https://doi.org/10.3390/atmos14030517

Zhang, Y., Li, J., & Liu, D. (2024). Spatial Downscaling of ERA5 Reanalysis Air Temperature Data Based on Stacking Ensemble Learning. *Sustainability*, *16*(5), 1934. https://doi.org/10.3390/su16051934

Zhao, L., Zhou, W., Peng, Y., Hu, Y., Ma, T., Xie, Y., Wang, L., Liu, J., & Liu, Z. (2021). A new AG-AGB estimation model based on MODIS and SRTM data in Qinghai Province, China. *Ecological Indicators*, *133*, 108378. https://doi.org/10.1016/j.ecolind.2021.108378

Zhao, J., Li, T., Shi, K., Qiao, Z., & Xia, Z. (2021). Evaluation of ERA-5 precipitable water vapor data in plateau areas: a case study of the northern Qinghai-Tibet Plateau. *Atmosphere*, *12*(10), 1367. https://doi.org/10.3390/atmos12101367

Zhu, L., Tian, H., Huang, N., Wang, L., & Niu, Z. (2024). Spatial-temporal variations of surface water area during 1986–2018 in Qinghai Province, northwestern China based on Google Earth Engine. *Big Earth Data*, *8*(2), 333–349. https://doi.org/10.1080/20964471.2023.2222945